Combined Torsional-Bending-Axial Dynamics of a Twisted Rotating Cantilever Timoshenko Beam With Contact-Impact Loads at the Free End

Sunil K. Sinha
Principal Engineer
GE Aircraft Engines,
M.D.: P-30,
General Electric Company,
1 Neumann Way,
Cincinnati, OH 45215
e-mail: sunil.sinha@ae.ge.com

In this paper, consideration is given to the dynamic response of a rotating cantilever twisted and inclined airfoil blade subjected to contact loads at the free end. Starting with the basic geometrical relations and energy formulation for a rotating Timoshenko beam constrained at the hub in a centrifugal force field, a system of coupled partial differential equations are derived for the combined axial, lateral and twisting motions which includes the transverse shear, rotary inertia, and Coriolis effects, as well. In the mathematical formulation, the torsion of the thin airfoil also considers a very general case of shear center not being coincident with the CG (center of gravity) of the cross section, which allows the equations to be used also for analyzing eccentric tip-rub loading of the blade. Equations are presented in terms of axial load along the longitudinal direction of the beam which enables us to solve the dynamic pulse buckling due to the tip being loaded in the longitudinal as well as transverse directions of the beam column. The Rayleigh–Ritz method is used to convert the set of four coupled-partial differential equations into equivalent classical mass, stiffness, damping, and gyroscopic matrices. Natural frequencies are computed for beams with varying "slenderness ratio" and "aspect ratio" as well as "twist angles." Dynamical equations account for the full coupling effect of the transverse flexural motion of the beam with the torsional and axial motions due to pretwist in the airfoil. Some transient dynamic responses of a rotating beam repeatedly rubbing against the outer casing is shown for a typical airfoil with and without a pretwist.
[DOI: 10.1115/1.2423035]

1 Introduction

Rotating beams, which have importance due to numerous practical usage such as jet engine blades, helicopter rotor blades, airplane propellers, satellite antennas, cutting-tool dynamics, and other turbomachinery applications, have been investigated for a long time. In order to analyze the dynamic characteristics of turbine and compressor blades, it is a common practice to consider it as a rotating radial cantilever beam. At the same time turbine and compressor blade designers have long felt that this characterization ignores some vital geometrical details of a real blade such as lean and twist in the blade; which limits the applicability of such simplified analytical models especially in the area of aerodynamic flutter and rub-induced dynamic instabilities in the blade. One such aspect with direct applications to turbine and compressor blades is the vibration of pretwisted beams, which is commonly referred as "twist-bend coupling characteristics of airfoils." During a typical rub-induced vibration event, the blade-tip moving with a tangential velocity of about 400–500 m/s makes a sudden glancing contact (impacting at a very shallow incidence angle) on the casing inner surface; which becomes the excitation mechanism for initiating free vibration in the blade. This process is repeated hundreds of times usually with one rub event every revolution. The typical radial interference between the blade tip and the casing inner surface responsible for generating the periodic contact rub load usually does not exceed 0.10–0.15 mm. After the earlier works [1–4] done about 30 years ago on free vibration characteristics of pretwisted beams simulating the airfoil, there is a considerable current interest in applying the methods of nonlinear vibration to the dynamic stability of asymmetric airfoils cross sections, especially rotating blades with aerodynamic excitations [5,6]. Dynamic stability of cantilever beams with varying levels of complexity and different types of loading conditions has been investigated by Chen and Peng [7], Hodges [8], Sinha [9], Chen and Ho [10], etc.

After the importance of transverse shear and rotary inertia in the beam formulation was shown by Timoshenko [11], many different aspects of his beam theory have been studied by several authors over the past 40 years. Leissa and Jacob [12] were the first ones to investigate the free vibration characteristics of cantilevered twisted beams and plates as a three-dimensional vibration problem. Rosen [13] has presented a comprehensive review of structural and dynamic aspects of pretwisted beams. Lin and his coworkers [14] have performed dynamic analysis of nonuniform pretwisted Timoshenko beam with elastic boundary conditions. Petrov and Geraldin [15] have developed the finite-element theory for a curved and twisted beams based upon a geometrically nonlinear formulation. Among the newer contributions, Tang and Yu [16] have presented a generalized variational principle on the nonlinear theory of a pretwisted curved beam. Other recent contributions in this field [17–22] primarily deal with the free vibration characteristics of the twisted rotating beams; which also include the effect of transverse shear and rotary inertia. Different parameters of dynamic stability of twisted rotating beams under external axial loads have been investigated by Chen and Keer [23], Lee [24], Liao and Huang [25], and Sakar and Sabuncu [26]. Yang and Tsao [27] studied the dynamic stability of pretwisted blade due to changing rotational speed. Temel [28,29] was the first one to analyze the transient response of a curved beam in the form of a helix and subjected to time-dependent loads. Turhan and Bulut [30]

Contributed by the Applied Mechanics Division of ASME for publication in the JOURNAL OF APPLIED MECHANICS. Manuscript received February 15, 2005; final manuscript received May 31, 2006. Review conducted by Marc P. Mignolet.

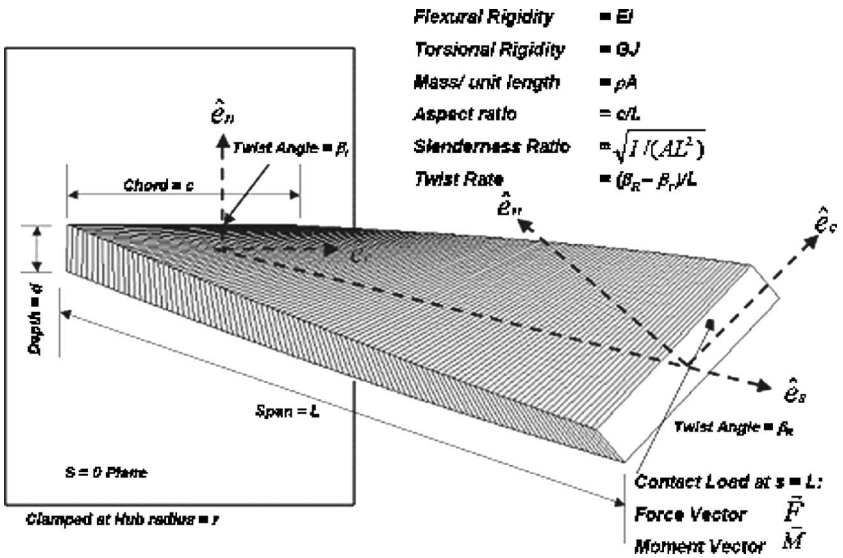

Fig. 1 A pretwisted Timoshenko beam and the local coordinate system

focused on the dynamic stability of a rotating blade due to fluctuations in the speed of the shaft. In the current work, our main focus is on developing the governing dynamical equations to analyze the effect of rub-induced contact-impact forces at the free end of the rotating blade modeled as a cantilever Timoshenko beam with a pretwist (see Fig. 1).

Starting from the basic deformation and velocity equations along with the rotary inertia and gyroscopic effect terms, a complete set of coupled dynamic equations has been derived for this problem. The eigenvalue problem of these equations in a matrix form is solved to determine the fundamental natural frequencies for a combination of varying geometrical parameters to characterize the Timoshenko beam. We have also solved the corresponding transient dynamics problem due to time-dependent contact-impact loading at the free end for twisted and untwisted blades.

2 Rotating Cantilever Timoshenko Beam Formulation for a Pretwisted Blade With Lean

For mathematical derivation, we consider that elastically deformable blades of outer radius "R" with the stagger angle "β_r," which the blade root-chord makes with the engine axis, are mounted on a rigid disk of hub radius "r" (see Fig. 2(a) and the Nomenclature for a full list of notations). We introduce two different local coordinate frames of reference attached to the rotating blade called "axial-tangential-radial" with unit vectors as $(\hat{e}_a, \hat{e}_t, \hat{e}_r)$ and, "chord-normal-span" with unit vectors as $(\hat{e}_c, \hat{e}_n, \hat{e}_s)$, respectively (see Fig. 2(b)) such that the longitudinal axis of the equivalent Timoshenko beam passes through the center of gravity (CG) of the beam cross section. The blade twist angle β is defined such that the airfoil center of curvature in a fan or compressor blade is towards the direction of rotation or spin-velocity Ω whereas in a turbine blade it is in the opposite direction of Ω. It should be noted that in general due to lean in the blade, the blade longitudinal axis in the span direction may not necessarily coincide with the local radial direction. Thus, the effect of the sweep angle α in a blade with a lean about the local radial direction is as follows:

$$\alpha > 0: \quad \text{forward-swept blade}$$

$$\alpha = 0: \quad \text{radial blade}$$

$$\alpha < 0: \quad \text{backward-swept blade}$$

In actual applications, the typical magnitude of the sweep-angle α is relatively small which ranges from -15 to about 15 deg. For such small values of α, one can assume that the normal to any beam cross-section surface makes a constant angle with the local radial direction $(\hat{e}_r)$ passing through the centroid of that cross section. In this analysis we further assume that due to twist in the beam, the "stagger angle $\beta(s)$" changes linearly as we move along the blade longitudinal axis from the root to the tip, such that

$$\beta(s) = \beta_r + s\beta' \tag{1}$$

and the rate of twist

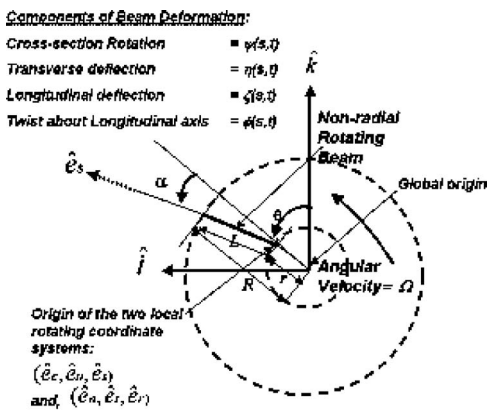

(*a*)

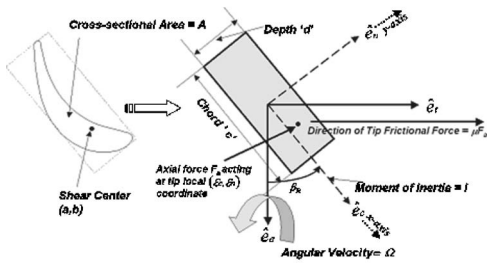

(*b*)

Fig. 2 (*a*) Schematic representation of an inclined rotating beam with respect to the fixed global frame of reference as viewed along the spin axis. (*b*) Airfoil cross section and its equivalent Timoshenko beam representation as viewed from the free end of the blade.

$$\beta' = \frac{\beta_R - \beta_r}{L} = \frac{(\beta_R - \beta_r)\cos\alpha}{(R-r)} \tag{2}$$

The individual blades behave like a cantilever beam column of span length "L" and are subjected to a centrifugal force field F_{cf} generated due to the rotor spin velocity "Ω," which for the derivation purposes can be treated as an external force on the system. Thus, the free end of the cantilever beam at $s=L$ is subjected to a generalized external force vector $\boldsymbol{\mathcal{F}}$ and moment vector $\boldsymbol{\mathcal{M}}$ such that

$$\begin{aligned}\boldsymbol{\mathcal{F}} &= F_C\hat{e}_c + F_N\hat{e}_n + F_S\hat{e}_s \\ \boldsymbol{\mathcal{M}} &= M_C\hat{e}_c + M_N\hat{e}_n + M_S\hat{e}_s\end{aligned} \tag{3}$$

The span direction component "F_S (+ sign: tension and − sign: compression)" of the external blade tip rub load vector $\boldsymbol{\mathcal{F}}$ acting along the longitudinal axis of the beam, henceforth is represented by F_a. The tip rub force F_a is a dynamic contact load, which is nonzero only during the tip travel through the rub zone on the stator and will always have a (−) sign due to the contact load being compressive in nature. The chord and normal (thickness direction) components F_C and F_N are generated when friction at the contact surfaces is also considered in the analysis. In the most general case, the tip-rub force F_a may be acting eccentrically at a point with its coordinate location as $(\varepsilon_c, \varepsilon_n)$ with respect to the CG of the beam cross section at the tip. For thick blades, the value of ε_n can be in the range of $[(-d/2) \geq \varepsilon_n \geq (d/2)]$ depending upon whether the blade is rubbing at the concave side or the convex side of the airfoil. For thin blades, $\varepsilon_n \approx 0$, and in the extreme case of tip rub at the edge of the beam cross section, we will have, $\varepsilon_c = \pm(c/2)$. In addition, the blade is deformed in bending by applying bending moment about its chord in such a way that a typical cross section of the deformed blade produces the cross-section rotation "ψ," the lateral deflection "η" at the neutral axis, the axial deflection "ζ" and the angle of twist as "ϕ." It is assumed that all four components of deformation are functions of spatial coordinate "s," measured along the beam axis and the temporal parameter time "t." It is also assumed that the minor principal moment of inertia of the blade cross-section "I" coincides with the chord direction so that under pure bending moment the blade lateral deflection $\eta(s,t)$ takes place in the direction normal to the chord with the neutral surface passing through the radial-chord plane.

For the analytical derivation, we will use the usual notations such as, elastic Young's modulus "E," Poisson's ratio "ν," shear modulus "$G=E/2(1+\nu)$," material mass density "ρ," and cross-sectional area "A." With respect to the stationary global cartesian unit vectors $(\hat{i},\hat{j},\hat{k})$, the local unit vectors attached to the beam $(\hat{e}_c,\hat{e}_n,\hat{e}_s)$, rotating at a constant angular velocity Ω such that $\theta=\Omega t$, are related to each other as

$$\begin{Bmatrix}\hat{e}_c\\ \hat{e}_n\\ \hat{e}_s\end{Bmatrix} = \begin{bmatrix}-\sin\beta\cos(\theta+\alpha) & \cos\beta & \sin\beta\sin(\theta+\alpha)\\ -\cos\beta\cos(\theta+\alpha) & -\sin\beta & \cos\beta\sin(\theta+\alpha)\\ \sin(\theta+\alpha) & 0 & \cos(\theta+\alpha)\end{bmatrix}\begin{Bmatrix}\hat{i}\\ \hat{j}\\ \hat{k}\end{Bmatrix} \tag{4}$$

It is assumed that any warping of the airfoil cross section caused by the torque varying along the span of the beam will be negligibly small. A typical airfoil cross section is not symmetrical about any of the principal axes and as such, in general, its "shear center" may not necessarily coincide with the centroid (CG) of the beam cross section. As a result, under the combined twisting and bending deformation of the airfoil, it is assumed that the shear center in the local coordinate system (chord-normal-span) is located at (a,b,s) in such a way that its position vector is described as

$$[a]\hat{e}_c + [b]\hat{e}_n + [s]\hat{e}_s \tag{5}$$

Then, with (a,b) as the shear center of the cross section and J_0 as the centroidal polar moment of inertia of the cross section, the effective polar moment of inertia for the twist motion can be written as

$$J_0 + A(a^2+b^2) \tag{6}$$

Here, we neglect the warping of the beam cross section and the slope $\eta_{,s}(s,t)$ of the transverse deformation of the beam is the sum of the rotation $\psi(s,t)$ and the rotation of the cross section due to shear force $Q(s,t)$ expressed as $-(Q/\kappa AG)$, i.e.

$$\eta_{,s}(s,t) = \psi(s,t) - \frac{Q(s,t)}{\kappa AG} \tag{7}$$

The angular velocity vector of the beam column due to spin velocity Ω is

$$[\Omega\cos\beta]\hat{e}_c + [-\Omega\sin\beta]\hat{e}_n + [0]\hat{e}_s \tag{8}$$

Under the small rotation assumptions, the rotation of the beam cross section after the deformation can be expressed as a rotation vector $\boldsymbol{\mathfrak{R}}$ such that

$$\boldsymbol{\mathfrak{R}} = [\psi]\hat{e}_c + [\phi]\hat{e}_s \tag{9}$$

Due to pretwist in the beam about the span axis (s-direction) with the twist rate of β', the derivative of the cross-section rotation vector term $\boldsymbol{\mathfrak{R}}$ is derived using the chain rule as

$$\frac{d\boldsymbol{\mathfrak{R}}}{ds} = \left[\frac{\partial\psi}{\partial s}\hat{e}_c + \psi\frac{\partial\hat{e}_c}{\partial s}\right] + \frac{\partial\phi}{\partial s}\hat{e}_s$$

i.e.

$$\frac{d\boldsymbol{\mathfrak{R}}}{ds} = [\psi_{,s}]\hat{e}_c + [\beta'\psi]\hat{e}_n + [\phi_{,s}]\hat{e}_s \tag{10}$$

In the above equation, $\psi_{,s}$ and $\beta'\psi$ represent the changes in the curvature of the beam about the chord and normal axes of the cross section due to bending about the two principal directions. In the derivative of the rotation vector $\boldsymbol{\mathfrak{R}}$ the contribution of the term containing unit vector component $\hat{e}_n$ is only due to pretwist in the beam. For example, in an untwisted beam with $\beta'=0$, a bending moment about $\hat{e}_c$ will not produce any curvature change about $\hat{e}_n$. The deformation vector of any point on the Timoshenko beam located at (x,y,s) in the local chord-normal-span coordinate system caused by the four components of deformation (ψ,η,ζ,ϕ) is obtained as

$$[-(y-b)\phi]\hat{e}_c + [\eta + (x-a)\phi]\hat{e}_n + [\zeta - y\psi]\hat{e}_s \tag{11}$$

The position vector in the local chord-normal-span coordinate system after deformation of any typical point at (x,y,s) can be written as

$$[x - y\phi + b\phi]\hat{e}_c + [y + (\eta - a\phi) + x\phi]\hat{e}_n + [s + \zeta - y\psi]\hat{e}_s \tag{12}$$

The time-dependent position vector of the rotating beam clamping point at the hub radius$=r$ in the global fixed frame of reference is $(r\sin\theta\hat{i} + r\cos\theta\hat{k})$. After some lengthy algebraic manipulation, the position vector of the clamping point in the local $(\hat{e}_c,\hat{e}_n,\hat{e}_s)$ system is expressed as

$$[r\sin\beta\sin\alpha]\hat{e}_c + [r\cos\beta\sin\alpha]\hat{e}_n + [r\cos\alpha]\hat{e}_s \tag{13}$$

Thus, the corresponding global position vector in the chord-normal-span coordinate system after deformation of a typical point at (x,y,s) on the beam can be written as

$$\begin{aligned}&[r\sin\beta\sin\alpha + x - y\phi + b\phi]\hat{e}_c + [r\cos\beta\sin\alpha + y + (\eta - a\phi)\\ &\quad + x\phi]\hat{e}_n + [r\cos\alpha + s + \zeta - y\psi]\hat{e}_s\end{aligned} \tag{14}$$

The time derivatives of the unit vectors $(\hat{e}_c,\hat{e}_n,\hat{e}_s)$ are obtained as

$$\dot{\hat{e}}_c = \Omega \sin\beta(s)\hat{e}_s$$
$$\dot{\hat{e}}_n = \Omega \cos\beta(s)\hat{e}_s \tag{15}$$
$$\dot{\hat{e}}_s = -\Omega \sin\beta(s)\hat{e}_c - \Omega \cos\beta(s)\hat{e}_n$$

Hence, the corresponding velocity vector $\boldsymbol{V}$ in a fixed global frame of reference, for any typical point on a rotating beam located at (x,y,s) with respect to the local $(\hat{e}_c,\hat{e}_n,\hat{e}_s)$ system, is derived as

$$\begin{aligned}\boldsymbol{V} = &\left\{\begin{bmatrix}\zeta_{,t} - y\psi_{,t} + (r\cos\beta\sin\alpha + y + \eta - a\phi + x\phi)\Omega\cos\beta\\ +(r\sin\beta\sin\alpha + x - y\phi + b\phi)\Omega\sin\beta\end{bmatrix}\sin\theta\right\}.\hat{i}\\ &+\left\{\begin{bmatrix}(s + r\cos\alpha + \zeta - y\psi)\Omega - \eta_{,t}\cos\beta\\ -(x\cos\beta - a\cos\beta - y\sin\beta + b\sin\beta)\phi_{,t}\end{bmatrix}\cos\theta\right\}\\ &-[(x\sin\beta - a\sin\beta + y\cos\beta - b\cos\beta)\phi_{,t} + \eta_{,t}\sin\beta].\hat{j}\\ &+\left\{\begin{bmatrix}\zeta_{,t} - y\psi_{,t} + (r\cos\beta\sin\alpha + y + \eta - a\phi + x\phi)\Omega\cos\beta\\ +(r\sin\beta\sin\alpha + x - y\phi + b\phi)\Omega\sin\beta\end{bmatrix}\cos\theta\right\}\\ &+\left\{-\begin{bmatrix}(s + r\cos\alpha + \zeta - y\psi)\Omega - \eta_{,t}\cos\beta\\ -(x\cos\beta - a\cos\beta - y\sin\beta + b\sin\beta)\phi_{,t}\end{bmatrix}\sin\theta\right\}.\hat{k}\end{aligned} \tag{16}$$

In a typical twisted beam formulation, it is a common practice to characterize the bending mode deformation about the two principal axes of the beam cross section (see the Appendix for details) as a coupled deflection in $(x-x)$ and $(y-y)$ directions, separately. In the present approach, we have introduced twist ϕ of the beam cross section about the longitudinal axis as an independent degree-of-freedom. Recalling that in a typical beam formulation inherent assumption of $I_{yy} \gg I_{xx}$ along with (a,b) being the shear center of a nonsymmetric cross section and J_0 its polar moment of inertia, we have $I_{xx}+I_{yy}=J_0+A(a^2+b^2)$ such that for shear center coincident with CG

$$I_{xx} = \int_{\text{Area}}\int y^2 dA = I, \quad I_{yy} = \int_{\text{Area}}\int x^2 dA \approx \infty \quad \text{and}$$
$$J_0 = \int_{\text{Area}}\int (x^2 + y^2)dA \tag{17}$$

The above relationship assumes that in an equivalent symmetrical cross section under combined twist and bending, the shear center would coincide with its centroid such that, $a=0$ and $b=0$. It is obvious that when the shear center is not coincident with the CG of the cross section, the contact forces will always generate a moment at the free end. We will recall that with the shear modulus $G=E/2(1+\nu)$, the torsional rigidity for a thin cross section can be written as "GJ" in which according to Timoshenko and Goodier [31] for rectangular cross sections, the torsion constant $J=(1/3)cd^3$. Since, the flexural bending in a pretwisted beam would inherently result in a twist-bend-coupling caused by the components of the beam deformation in the two principal directions of the cross section, it is convenient to represent the flexural rigidity term "EI_{yy}" as a function of its torsional rigidity term GJ. In addition, in such beams with thin cross sections the effect of Poisson's ratio ν is negligible and as such the flexural rigidity about the major principal axis EI_{yy} in terms of its torsional rigidity GJ can be approximated as

$$EI_{yy} \approx (2GJ - EI) \tag{18}$$

Thus, combining the kinetic energy "T" and the potential energy "U" due to bending, transverse shear, twisting and centrifugal loads "F_{cf}" as well as the axial force due to contact "F_a" yields the simplified form of Lagrangian "Λ" for the rotating Timoshenko's beam column as

$$\begin{aligned}\Lambda = T - U = \frac{1}{2}\int_0^L \Bigg[&\rho A\left(\begin{bmatrix}\zeta_{,t} - y\psi_{,t} + (r\cos\beta_r\sin\alpha + y + \eta - a\phi + x\phi)\Omega\cos\beta\\ +(r\sin\beta_r\sin\alpha + x - y\phi + b\phi)\Omega\sin\beta\end{bmatrix}^2\right.\\ &\left.+\left\{(s + r\cos\alpha + \zeta - y\psi)\Omega - \eta_{,t}\cos\beta - \begin{bmatrix}(x-a)\cos\beta\\ -(y-b)\sin\beta\end{bmatrix}\phi_{,t}\right\}^2\right)\\ &\{[(x-a)\sin\beta + (y-b)\cos\beta]\phi_{,t} + \eta_{,t}\sin\beta\}^2\\ &-\begin{bmatrix}EI(\psi_{,s})^2 + (2GJ - EI)(\beta'\psi)^2 + GJ(\phi_{,s})^2 + AE(\zeta_{,s})^2\\ +\kappa AG(\eta_{,s} - \psi)^2 + \kappa AG(\beta'\eta)^2 + 2\kappa AG\beta'(y-b)\phi(\eta_{,s} - \psi)\\ +2(2GJ - EI)\beta'\phi_{,s}[\psi + (y-b)\psi_{,s}]\end{bmatrix}\\ &-F_a\{[(\eta + (x-a)\phi)_{,s}]^2 + [\beta'\eta]^2 + [(y-b)\phi_{,s}]^2\}\\ &-F_{cf}\cos\alpha\{[(\eta + (x-a)\phi)_{,s}]^2 + [(y-b)\phi_{,s}]^2\} + 2\mu F_a\cos\beta_R\psi\zeta_{,s}\\ &+2F_a[(a-\varepsilon_c)\cos\beta'(s-L) + (b-\varepsilon_n)\sin\beta'(s-L)]\psi\phi_{,s}\\ &-2F_a[(b-\varepsilon_n)\cos\beta'(s-L) - (a-\varepsilon_c)\sin\beta'(s-L)]\beta'(\eta-b)\phi_{,s}\Bigg] ds\end{aligned} \tag{19}$$

The Lagrangian equation is

$$\frac{d}{dt}\left(\frac{\partial \Lambda}{\partial x_{i,t}}\right) - \frac{\partial \Lambda}{\partial x_i} + \frac{d}{ds}\left(\frac{\partial \Lambda}{\partial x_{i,s}}\right) = R_i \tag{20}$$

Using the Lagrangian Λ in the Lagrange's equation yields the following 4 coupled partial differential equations of motion for ψ, η, ζ, and ϕ, respectively, in a local frame of reference attached to the rotating beam-column with angular velocity Ω as

(a) Bending moment balance due to rotation of the beam cross section about its minor principal axis (chord)

$$\begin{aligned} &-EI\psi_{,ss} - \kappa AG(\eta_{,s} - \psi) + (2GJ - EI)\beta'(\beta'\psi + \phi_{,s} + b\phi_{,ss}) + \kappa AG\beta' b\phi \\ &- F_a[(a-\varepsilon_c)\cos\beta'(s-L) + (b-\varepsilon_n)\sin\beta'(s-L)]\phi_{,s} - \mu F_a \cos\beta_R \zeta_{,s} \\ &- \rho I\Omega^2\psi + \rho I\dot{\Omega}\sin\beta\phi + \rho I\psi_{,tt} + 2\rho I\Omega\sin\beta\phi_{,t} = T_c(s,t) \end{aligned} \tag{21a}$$

(b) Shear force balance in the normal direction through the cross section of the beam

$$\begin{aligned} &-\kappa AG[\eta_{,ss} - \psi_{,s}] + \kappa AG\beta' b\phi_{,s} + \kappa AG(\beta')^2\eta - F_a[\eta_{,ss} - (\beta')^2\eta - a\phi_{,ss}] \\ &+ F_a[(b-\varepsilon_n)\cos\beta'(s-L) - (a-\varepsilon_c)\sin\beta'(s-L)]\beta'\phi_{,s} - F_{\mathrm{cf}}\cos\alpha[\eta_{,ss} - a\phi_{,ss}] \\ &- \rho A\dot{\Omega}\cos\beta\zeta - \rho A\Omega^2\cos\beta[\cos\beta(\eta - a\phi) + b\sin\beta\phi] \\ &- 2\rho A\Omega\cos\beta\zeta_{,t} + \rho A\eta_{,tt} - \rho Aa\phi_{,tt} = Q_n(s,t) \end{aligned} \tag{21b}$$

(c) Axial force balance due to membrane stretching along the neutral surface of the beam

$$\begin{aligned} &-EA\zeta_{,ss} - \rho A\Omega^2\zeta + \rho A\dot{\Omega}[\cos\beta(\eta - a\phi) + b\sin\beta\phi] + \mu F_a\cos\beta_R\psi_{,s} \\ &+ \rho A[\zeta_{,tt} + 2\Omega\cos\beta\eta_{,t} - 2\Omega(a\cos\beta - b\sin\beta)\phi_{,t}] = Q_s(s,t) \end{aligned} \tag{21c}$$

(d) Torque balance due to twist in the beam (neglecting the warping of the cross section)

$$\begin{aligned} &-GJ\phi_{,ss} + \rho I\dot{\Omega}\sin\beta\psi + \rho I\Omega^2\sin^2\beta\phi - \kappa AG\beta' b(\eta_{,s} - \psi) \\ &-(2GJ - EI)\beta'(\psi_{,s} - b\psi_{,ss}) - [F_a + F_{\mathrm{cf}}\cos\alpha][(J_0/A)\phi_{,ss} - a\eta_{,ss}] \\ &+ F_a[(a-\varepsilon_c)\cos\beta'(s-L) + (b-\varepsilon_n)\sin\beta'(s-L)][(\beta')^2\eta + \psi_{,s}] \\ &- F_a[(b-\varepsilon_n)\cos\beta'(s-L) - (a-\varepsilon_c)\sin\beta'(s-L)]\beta'(\eta_{,s} - \psi) \\ &+ \rho J_0\phi_{,tt} - \rho Aa\eta_{,tt} + \rho A(a^2 + b^2)\phi_{,tt} - 2\rho I\Omega\sin\beta\psi_{,t} + 2\rho A\Omega(a\cos\beta - b\sin\beta)\zeta_{,t} \\ &= T_s(s,t) \end{aligned} \tag{21d}$$

In the above equations, $Q_n(s,t)$ and $Q_s(s,t)$ account for the distributed lateral loads on the beam column in the thickness (normal) and in the longitudinal (span) directions, respectively. Similarly, $T_n(s,t)$ and $T_s(s,t)$ account for the distributed bending and twist moments on the beam column about the neutral (chord) axis and longitudinal (span) directions, respectively. These distributed external force and moments are caused due to centrifugal loads, nonconstant spin-velocity and gas loads due to fluid flow over the surface of the blade. For example, due to radial lean in the blade by an angle α the centrifugal load acting at the CG of the beam cross section generates distributed transverse forces and twist moments given by

$$Q_n(s,t) = \rho A\Omega^2(s + r\cos\alpha)\sin\alpha\cos(\beta_r + \beta' s) \tag{22}$$

$$T_s(s,t) = \rho A\Omega^2(s + r\cos\alpha)\sin\alpha[b\cos(\beta_r + \beta' s) - a\sin(\beta_r + \beta' s)] \tag{23}$$

Obviously, in a free-vibration problem, all nonhomogeneous terms on the right-hand side of the above set of equations are set to zero. The presence of the axial-force term F_a acting on the free end of the beam in these equations contributes to the lateral as well as torsional buckling of the Timoshenko beam. In the above equations, it should be noted that in a rotating beam; its lateral motion $\eta(s,t)$ is coupled with the longitudinal motion $\zeta(s,t)$ and its cross section rotation $\psi(s,t)$ is coupled with the twist in the beam $\phi(s,t)$. These couplings are due to Coriolis effects in the dynamical system, which introduce velocity-dependent skew-symmetric terms in the equations of motion. In a dynamics problem, F_a would become a function of time t and can be expressed as $F_a = F(t)$. If $F(t)$ is an oscillating force with a pulse frequency of $f_p - Hz$, it develops a parametric excitation in the system which in a sinusoidal form is written as

$$F_a = F(t) = F_{\max}\cos(2\pi f_p t) \tag{24}$$

The set of four partial differential equations outlined in Eqs. (21*a*)–(21*d*) describe the fully coupled dynamical characteristics of a twisted rotating cantilever Timoshenko beam with axial loading at the free end, which also includes the effects of nonconstant rotational speed as well as the Coriolis forces. This is the first attempt in any published literature to formulate the complex set of equations in its entirety. The simpler forms of these equations used by other researchers can easily be derived by setting certain parameters equal to zero, such as by making $\dot{\Omega} = 0$, these equations represent the dynamics of a beam rotating at a constant speed. Previous derivations for the cantilever airfoil vibration in coupled torsional-bending mode reported in the literature [1–4] are simplified using Euler–Bernoulli beam formulation with $\dot{\Omega} = 0$, $a = 0$, $b = 0$, and $F_a = 0$. Furthermore, by setting the sweep or the radial lean angle $\alpha = 0$, one obtains the equations for a radial rotating beam. Similarly, by setting the axial loading term $F_a = 0$, the corresponding equations for the free vibrations of a beam are obtained. The contributions of axial motion can be disregarded by dropping the terms containing ζ due to additional degree-of-freedom in the longitudinal direction of the beam. In addition, by setting the twist parameter $\beta' = 0$, one can simplify the equations similar to one used by Lin [19] for a beam with a constant stagger angle. Similarly, by setting the hub radius term $r = 0$, one can derive the equations similar to one used by Oguamanam and Heppler [18]. These equations can be further simplified to represent

the coupled flexural and torsional vibrations of classical Euler–Bernoulli's beam as shown by Timoshenko et al. [11]. It has been verified that the coupled flexural and torsional elastic buckling equation due to axial forces and end moments also reduce to the form similar to one derived by Timoshenko and Gere [32]. On replacing the torsional rigidity term GJ by the relations expressed in Eq. (18) one obtains a set of equations similar to that used by Banerjee [21].

3 Boundary Conditions and External Forces

The geometric boundary conditions for the Timoshenko's beam under consideration with four components of deformation $(\psi, \eta, \zeta, \phi)$ are as follows:

$$\psi(0,t) = 0, \quad \eta(0,t) = 0, \quad \zeta(0,t) = 0 \quad \phi(0,t) = 0 \tag{25}$$

The corresponding four natural boundary conditions at the free end of the cantilever beam for $(s=L)$ are expressed in terms of the contact force vector $\boldsymbol{\mathcal{F}}$ and moment vector $\boldsymbol{\mathcal{M}}$ components (see Eq. (3)) as

$$F_C = 0, \quad M_N = 0 \tag{26}$$

$$(\text{bending moment})_{\text{at } s=L} = M_C = EI\psi_{,s}|_{s=L} = F_a[\varepsilon_n + \varepsilon_c \sin(\beta' L)] \tag{27}$$

$$(\text{shear force})_{\text{at } s=L} = F_N = -\kappa AG[\eta_{,s} - \psi]_{s=L} = -\mu F_a \cos\beta_R \tag{28}$$

$$(\text{axial force})_{\text{at } s=L} = F_S = EA\zeta_{,s}|_{s=L} = F_a \tag{29}$$

$$(\text{torque})_{\text{at } s=L} = M_S = GJ\phi_{,s}|_{s=L} = \mu F_a[(\varepsilon_c - a)\cos\beta_R - (\varepsilon_n - b)\sin\beta_R] \tag{30}$$

In a contact-dynamics problem, the tip load F_a along the longitudinal axis and its point of application on the beam cross section $(\varepsilon_c, \varepsilon_n)$ will be time dependent. If the outer case radial tip-clearance γ and its radial stiffness K_{case} need to be included in the analysis then

$$F_a = 0 \quad \text{for } \{\cos\alpha\zeta + \cos\beta_R \sin\alpha[\eta + (\varepsilon_c - a)\phi]\}|_{s=L} < \gamma \tag{31}$$

$$\text{and} \quad F_a = -K_{\text{case}}\{\cos\alpha\zeta + \cos\beta_R \sin\alpha[\eta + (\varepsilon_c - a)\phi] - \gamma\}|_{s=L}$$

$$\text{for} \quad \{\cos\alpha\zeta + \cos\beta_R \sin\alpha[\eta + (\varepsilon_c - a)\phi]\}|_{s=L} \geq \gamma \tag{32}$$

In order to account for the torsional deformation in the blade in Eq. (31), the positive sign on the chord is used, if the tip leading edge of the blade is rubbing and a negative sign is used if the tip trailing edge is in contact. It should be obvious that for the contact load at the mid-point of the tip cross section, the contribution from the twist parameter ϕ would be zero. The external tip forces $\boldsymbol{\mathcal{F}}$ and moments $\boldsymbol{\mathcal{M}}$ at the free-end of the beam act like point loads at $s=L$, and as such mathematically with the use of Dirac's Delta function $\delta(s-L)$ can be treated like a continuous or distributed external force, which are written as

$$T_c(s,t) = F_a[\varepsilon_n + \varepsilon_c \sin(\beta' L)]\delta(s-L) \tag{33a}$$

$$Q_n(s,t) = -\mu F_a \cos\beta_R \delta(s-L) \tag{33b}$$

$$Q_s(s,t) = F_a \delta(s-L) \tag{33c}$$

$$T_s(s,t) = \mu F_a[(\varepsilon_c - a)\cos\beta_R - (\varepsilon_n - b)\sin\beta_R]\delta(s-L) \tag{33d}$$

4 Rayleigh–Ritz Method and Ordinary Differential Equations of Motion in Matrix Form

One can use several different methods such Galerkin's or other weighted-residual techniques to convert the set of partial differential Eqs. (21*a*)–(21*d*) in a set of ordinary differential equations. Each technique imposes certain necessary boundary condition requirements on the approximating functions. Here, we have employed the classical Rayleigh–Ritz method for this purpose, which requires that as a necessary condition, the approximating function must satisfy the geometric constraints arbitrarily but the force-dependent natural boundary conditions may be relaxed. In the ideal situation, they may satisfy all the geometric as well as force boundary conditions of the present problem, however, it is not necessary in general. If the approximating functions do not satisfy all the force boundary conditions as well, then the integrated sum of the unbalanced weighted-residual force and moment terms must be set to zero at the free end. Thus, under these conditions, the solution of the above set of equations can be assumed as

$$\phi(s,t) = \sum_{j=0}^{\infty} U_j(s)W_j(t) = \sum_{j=1}^{\infty} [\sin\varphi_j s]W_j(t) \tag{34}$$

$$\psi(s,t) = \sum_{j=0}^{\infty} U_j(s)X_j(t) = \sum_{j=1}^{\infty} [\sin\varphi_j s]X_j(t) \tag{35}$$

$$\eta(s,t) = \sum_{j=0}^{\infty} V_j(s)Y_j(t) = \sum_{j=1}^{\infty} \frac{[1-\cos\varphi_j s]}{\varphi_j} Y_j(t) \tag{36}$$

$$\zeta(s,t) = \sum_{j=0}^{\infty} S_j(s)Z_j(t) = \sum_{j=1}^{\infty} \left[\frac{\sin\varphi_j s}{\varphi_j}\right] Z_j(t) \tag{37}$$

where

$$\varphi_j = \frac{(2j-1)\pi}{2L}$$

Hence, in order to apply the Rayleigh–Ritz's method, we substitute the assumed deflection shape functions in such a way that the shape function terms have proper dimensions of either length or slope (radians) as necessary. In the above sets of equations, the spatial derivative terms can be written as a function of a set of differential operators. In addition, the discretized form of Eqs. (21*a*)–(21*d*) is complete only when all the terms in the infinite series for the displacement functions $S_j(s)$, $U_j(s)$, and $V_j(s)$ are considered, however, in a numerical technique they must be truncated after a certain number of terms in the sequence. On applying the Rayleigh–Ritz's method with the assumed displacement functions, one obtains a set of ordinary differential equations in terms of time-dependent variables. The complete equations with the homogeneous as well as external force terms of these equations in a matrix form can be written as

$$\boldsymbol{M}\{\ddot{f}(t)\} + \boldsymbol{C}\{\dot{f}(t)\} + \boldsymbol{K}\{f(t)\} = \{P(t)\} \tag{38}$$

Here $\boldsymbol{M}$ is the coefficient matrix for the acceleration-dependent force terms generally known as inertia or the mass matrix, $\boldsymbol{C}$ is the coefficient matrix for the velocity-dependent force terms which can be due to damping or due to gyroscopic effects in the dynamical system, and $\boldsymbol{K}$ is the coefficient matrix for the displacement-dependent force terms generally known as the stiffness matrix. It can be seen that in Eq. (38) the terms containing generalized coordinates in the column-vector $\{f(t)\}$ are X, Y, Z, and $W's$, which are dimensionless. Suppose, we consider "N" number of terms for each of the four basic deformation trial functions outlined in Eqs. (33)–(36), then for brevity we can introduce following notations in lieu of the generalized coordinates $\{f(t)\}$

$$\begin{bmatrix} \boldsymbol{M} & \end{bmatrix}\begin{Bmatrix} \{\ddot{X}\}_N \\ \{\ddot{Y}\}_N \\ \{\ddot{Z}\}_N \\ \{\ddot{W}\}_N \end{Bmatrix} + \begin{bmatrix} \boldsymbol{C} & \end{bmatrix}\begin{Bmatrix} \{\dot{X}\}_N \\ \{\dot{Y}\}_N \\ \{\dot{Z}\}_N \\ \{\dot{W}\}_N \end{Bmatrix} + \begin{bmatrix} \boldsymbol{K} & \end{bmatrix}\begin{Bmatrix} \{X\}_N \\ \{Y\}_N \\ \{Z\}_N \\ \{W\}_N \end{Bmatrix} = \begin{Bmatrix} P(t) & \\ & \\ & \end{Bmatrix}_{4N} \tag{39}$$

It is obvious that with the N number of terms used to represent each of the four displacement functions viz. $(\psi, \eta, \zeta, \phi)$, the total number of degrees of freedom in the numerical scheme will be "$4N$." In the above equation, the right-hand side column-vector $\{P(t)\}$ representing all the external forces due to contact load F_a acting along the beam-axis eccentrically at $(\varepsilon_c, \varepsilon_n)$ in the chord-normal-plane at the free end of the cantilever beam column can be expressed as

$$\{P(t)\} = \begin{Bmatrix} \{P^{\psi}(t)\}_N \\ \{P^{\eta}(t)\}_N \\ \{P^{\zeta}(t)\}_N \\ \{P^{\phi}(t)\}_N \end{Bmatrix} = \begin{Bmatrix} \{F_a[\varepsilon_n + \varepsilon_c \sin(\beta' L)]U(L)\} \\ \{-\mu F_a \cos\beta_R V(L)\} \\ \left[\rho A\Omega^2 \int_0^L (s + r\cos\alpha) S ds + F_a S(L)\right]_N \\ \{\mu F_a[(\varepsilon_c - a)\cos\beta_R - (\varepsilon_n - b)\sin\beta_R]U(L)\} \end{Bmatrix} \tag{40}$$

Furthermore, the matrix terms used in Eq. (38) can be broken into following separate matrices

$$\boldsymbol{M}\{\ddot{f}(t)\} + [\boldsymbol{C}_D + \boldsymbol{C}_G]\{\dot{f}(t)\} + [\boldsymbol{K}_S + \boldsymbol{K}_F + \boldsymbol{K}_\Omega]\{f(t)\} = \{P(t)\} \tag{41}$$

where $\boldsymbol{M}$ is the mass matrix (symmetric), a function of density ρ and I, $\boldsymbol{K}_S$ is the elastic stiffness matrix (symmetric), a function of E, G, I, etc., $\boldsymbol{K}_\Omega$ is the centrifugal stress-related stiffness-matrix as a result of spin-velocity Ω (symmetric), $\boldsymbol{K}_F$ is the in-plane force-dependent circulatory matrix due to contact force F_a acting along the longitudinal axis at $(\varepsilon_c, \varepsilon_n, L)$ of the beam-column (nonsymmetric), $\boldsymbol{C}_D$ is the damping matrix due to the material internal damping $=(2\chi/\Omega)\boldsymbol{K}_s$, $\boldsymbol{C}_G(\Omega)$ is the gyroscopic matrix (skew symmetric), causes coupling of axial and lateral motions in the beam, and $\{P(t)\}$ is the column vector containing external forces on the dynamical system.

Thus, the individual nonzero terms in the equivalent mass $\boldsymbol{M}$, damping $\boldsymbol{C}$ and stiffness $\boldsymbol{K}$ matrices are as follows:

$$[Ki,j] = -EI\int_0^L U_i U_j'' ds + \kappa AG\int_0^L U_i U_j ds + (2GJ - EI)(\beta')^2 \int_0^L U_i U_j ds - \rho I\Omega^2 \int_0^L U_i U_j ds \tag{42}$$

$$[M_{i,j}] = \rho I \int_0^L U_i U_j ds \tag{43}$$

$$[K_{i,j+N}] = -\kappa AG \int_0^L U_i V_j' ds \tag{44}$$

$$[K_{i,j+2N}] = -\mu F_a \cos\beta_R \left[\int_0^L U_i S_j' ds\right] \tag{45}$$

$$[K_{i,j+3N}] = (2GJ - EI)\beta' \left[\int_0^L U_i U_j' ds - U_i(L)U_j(L)\right] + \kappa AG\beta' b \int_0^L U_i U_j ds + (2GJ - EI)\beta' b \left[\int_0^L U_i U_j'' ds\right] + \rho I\dot{\Omega} \int_0^L \sin\beta U_i U_j ds - F_a \left[\int_0^L [(a - \varepsilon_c)\cos\beta'(s - L) + (b - \varepsilon_n)\sin\beta'(s - L)]U_i U_j' ds - (a - \varepsilon_c)U_i(L)U_j(L)\right] \tag{46}$$

$$[C_{i,j+3N}] = 2\rho I\Omega \int_0^L \sin\beta U_i U_j ds \tag{47}$$

$$[K_{i+N,j}] = \kappa AG \left[\int_0^L V_i U_j' ds - V_i(L)U_j(L)\right] \tag{48}$$

$$[K_{i+N,j+N}] = -\kappa AG\left[\int_0^L V_i V_j'' ds - V_i(L)V_j'(L)\right] - \rho A\Omega^2 \int_0^L \cos^2\beta V_i V_j ds - \frac{\rho A\Omega^2}{2}\cos\alpha \int_0^L (R^2 - s^2\cos^2\alpha - r^2 - 2sr\cos\alpha)V_i V_j'' ds + (\beta')^2 \kappa AG \int_0^L V_i V_j ds - F_a\left[\int_0^L V_i V_j'' ds - V_i(L)V_j'(L) - (\beta')^2 \int_0^L V_i V_j ds\right] \tag{49}$$

$$[M_{i+N,j+N}] = \rho A \int_0^L V_i V_j ds \tag{50}$$

$$[K_{i+N,j+2N}] = -\rho A\dot{\Omega} \int_0^L \cos\beta V_i S_j ds \tag{51}$$

$$[C_{i+N,j+2N}] = -2\rho A\Omega \int_0^L \cos\beta V_i S_j ds \tag{52}$$

$$[K_{i+N,j+3N}] = (\kappa AG\beta' b)\left[\int_0^L V_i U_j' ds - V_i(L)U_j(L)\right] - \rho A\Omega^2 \int_0^L \cos\beta(b\sin\beta - a\cos\beta)V_i U_j ds + a\cos\alpha \frac{\rho A\Omega^2}{2}\int_0^L (R^2 - s^2\cos^2\alpha - r^2 - 2sr\cos\alpha)V_i U_j'' ds - F_a \begin{Bmatrix} -a\left[\int_0^L V_i U_j'' ds - V_i(L)U_j'(L)\right] \\ -\beta'\int_0^L [(b-\varepsilon_n)\cos\beta'(s-L) - (a-\varepsilon_c)\sin\beta'(s-L)]V_i U_j' ds + \beta'(b-\varepsilon_n)V_i(L)U_j(L) \end{Bmatrix} \quad (53)$$

$$[M_{i+N,j+3N}] = -\rho Aa\int_0^L V_i U_j ds \quad (54)$$

$$[K_{i+2N,j}] = \mu F_a \cos\beta_R\left[\int_0^L S_i U_j' ds\right] \quad (55)$$

$$[K_{i+2N,j+N}] = \rho A\dot{\Omega}\int_0^L \cos\beta S_i V_j ds \quad (56)$$

$$[C_{i+2N,j+N}] = 2\rho A\Omega\int_0^L \cos\beta S_i V_j ds \quad (57)$$

$$[K_{i+2N,j+2N}] = -EA\left[\int_0^L S_i S_j'' ds - S_i(L)S_j'(L)\right] - \rho A\Omega^2\int_0^L S_i S_j ds \quad (58)$$

$$[M_{i+2N,j+2N}] = \rho A\int_0^L S_i S_j ds \quad (59)$$

$$[K_{i+2N,j+3N}] = -\rho A\dot{\Omega}\int_0^L (a\cos\beta - b\sin\beta)S_i U_j ds \quad (60)$$

$$[C_{i+2N,j+3N}] = -2\rho A\Omega\int_0^L (a\cos\beta - b\sin\beta)S_i U_j ds \quad (61)$$

$$[K_{i+3N,j}] = -(2GJ - EI)\beta'\left[\int_0^L U_i U_j' ds\right] + (2GJ - EI)\beta' b\left[\int_0^L U_i U_j'' ds\right] + \kappa AG\beta' b\int_0^L U_i U_j ds + \rho I\dot{\Omega}\int_0^L \sin\beta U_i U_j ds - F_a \begin{Bmatrix} -\int_0^L [(a-\varepsilon_c)\cos\beta'(s-L) + (b-\varepsilon_n)\sin\beta'(s-L)]U_i U_j' ds + (a-\varepsilon_c)U_i(L)U_j(L) \\ +\beta'\int_0^L [(b-\varepsilon_n)\cos\beta'(s-L) - (a-\varepsilon_c)\sin\beta'(s-L)]U_i U_j ds \end{Bmatrix} \quad (62)$$

$$[C_{i+3N,j}] = -2\rho I\Omega\int_0^L \sin\beta U_i U_j ds \quad (63)$$

$$[K_{i+3N,j+N}] = -\kappa AG\beta' b\int_0^L U_i V_j' ds + \cos\alpha\frac{\rho aA\Omega^2}{2}\int_0^L (R^2 - s^2\cos^2\alpha - r^2 - 2sr\cos\alpha)U_i V_j'' ds - F_a \begin{Bmatrix} \beta'\int_0^L [(b-\varepsilon_n)\cos\beta'(s-L) - (a-\varepsilon_c)\sin\beta'(s-L)]U_i V_j' ds - \beta'(b-\varepsilon_n)U_i(L)V_j(L) \\ -(\beta')^2\int_0^L [(a-\varepsilon_c)\cos\beta'(s-L) + (b-\varepsilon_n)\sin\beta'(s-L)]U_i V_j ds - a\int_0^L U_i V_j'' ds \end{Bmatrix} \quad (64)$$

$$[M_{i+3N,j+N}] = -\rho Aa\int_0^L U_i V_j ds \quad (65)$$

$$[C_{i+3N,j+2N}] = 2\rho A\Omega\int_0^L (a\cos\beta - b\sin\beta)U_i S_j ds \quad (66)$$

$$[K_{i+3N,j+3N}] = -GJ\int_0^L U_i U_j'' ds + \rho I\Omega^2\int_0^L \sin^2\beta U_i U_j ds - \cos\alpha\frac{J_0\rho\Omega^2}{2}\int_0^L (R^2 - s^2\cos^2\alpha - r^2 - 2sr\cos\alpha)U_i U_j'' ds - F_a(J_0/A)\int_0^L U_i U_j'' ds \quad (67)$$

$$[M_{i+3N,j+3N}] = \rho J_0 \int_0^L U_i U_j ds + \rho A(a^2 + b^2) \int_0^L U_i U_j ds \quad (68)$$

All the terms of the matrices $\boldsymbol{M}$, $\boldsymbol{C}$, and $\boldsymbol{K}$ for a given beam dimension and the assumed displacement functions outlined in Eq. (38) can easily be determined by routine numerical integration method such as Simpson's rule. It should be noted that due to pretwist in the beam, we have kept all sine and cosine functions of the twist angle β inside the integration sign. During the spanwise integration of terms in the matrices, we determine the local value of $\beta(s)$ by the relationship described in Eq. (1) as

$$\beta(s) = \beta_r + s\beta' \quad (69)$$

Additionally, it can be seen that the rate of angular acceleration $\dot{\Omega}$ enters into the equations as the stiffness term. The above nonzero terms in the velocity-dependent coefficient matrix $[C_{i,j}]$ are all due to spin velocity Ω and represent the gyroscopic effect in the system by being skew symmetric in nature, which in the governing equations are shown as $\boldsymbol{C}_G$. The material internal damping can be taken into account as a function of the nondimensional factor χ of the critical damping of the beam material and the spin angular velocity Ω. In this situation, the typical terms in the damping matrix $[C_{i,j}]_D$ due to the material internal damping are computed as functions of stiffness matrix terms $[K_{i,j}]_S$ containing material parameters Young's modulus E and shear modulus G as well as shear coefficient κ of the beam, which are written as

$$[C_{i,j}]_D = \frac{2\chi}{\Omega}[K_{i,j}]_S \quad (70)$$

5 Sample Results of Fundamental Frequencies

The corresponding $\boldsymbol{M}$ and $\boldsymbol{K}$ matrices have been used for determining the nondimensional natural frequency term ξ by solving the following eigenvalue problem:

$$\boldsymbol{M}\{\ddot{f}(t)\} + [\boldsymbol{K}_S + \boldsymbol{K}_\Omega]\{f(t)\} = \{0\} \quad (71)$$

where nondimensional frequency parameter ξ is defined such that

$$\text{Natural frequency } \omega_N = \frac{\xi}{L^2}\sqrt{\frac{EI}{\rho A}} \text{ rad/s} \quad (72)$$

The eigenvalue solution of Eq. (71) yields natural frequencies both for rotating as well as nonrotating ($\Omega = 0, \boldsymbol{K}_\Omega = 0$) conditions of the beam. It should be recognized that there is a scarcity of published data with all the parameters considered in the current analytical model, such as a blade rotating with an angular velocity Ω, radial lean α, initial twist $(\beta_R - \beta_r)$, coefficient of friction μ, longitudinal load F_a and its eccentricity $(\varepsilon_c, \varepsilon_n)$, etc. Thus, in order to demonstrate the accuracy of the present method, we have compared the finite-element results and other limited amount of published data with the natural frequency values yielded by the much simplified versions of the current model.

5.1 Current Model Validation With Finite-Element Results. In an attempt to validate the present model for its frequency response, the analytically predicted frequencies are compared with the finite-element results for a typical low-pressure compressor blade with the following parameters:

L	= span length of the airfoil (beam)	=15.8 cm
c/L	=aspect ratio	=0.43
M	= mass of the airfoil (ρAL)	=120 gm
α	= angle of lean with respect to radius	=0
I	= moment of inertia of the cross section (airfoil)	=0.04213 cm^4
E	= elastic Young's modulus of the beam material	=117 G Pa
ρ	= beam mass material density	=4.466 gm/cm^3
$(\beta_R - \beta_r)$	= total twist in the blade	=−25°
Ω	= angular velocity of rotation (40 Hz)	=251.327 rad/s

Here, the finite-element (FE) model (shown in Fig. 3) was analyzed using a commonly used commercial code called ANSYS. In the FE model in order to ensure that the shear deformation effect is included, we have used three brick elements through the airfoil thickness.

For this particular blade, the first five vibrational mode finite-element computed frequencies have been compared with those determined by the current model and are shown in Table 1 for the stationary condition and blades rotating at 2400 rpm, respectively. As one can see that the correlation for the first five modes with the FE model is very good with the maximum error limited to 3.32%.

5.2 Comparison of Current Model With Other Published Data. We have also verified the current analytical model with the results reported in published literature by other researchers as well. Using the pretwisted Timoshenko beam finite-element approach Yardimoglu and Yildirim [20] have computed the frequencies for the first four modes for a blade with the span-length $L = 15.24$ cm, chord $c = 2.54$ cm, depth $d = 0.17272$ cm, and a total twist of $(\beta_R - \beta_r) = 45$ deg. The material properties for this blade such as, Young's modulus of elasticity and the mass density are $E = 206.85$ G Pa and $\rho = 7.8576$ gm/cm^3, respectively. The frequencies reported by Yardimoglu and Yildirim for this blade and

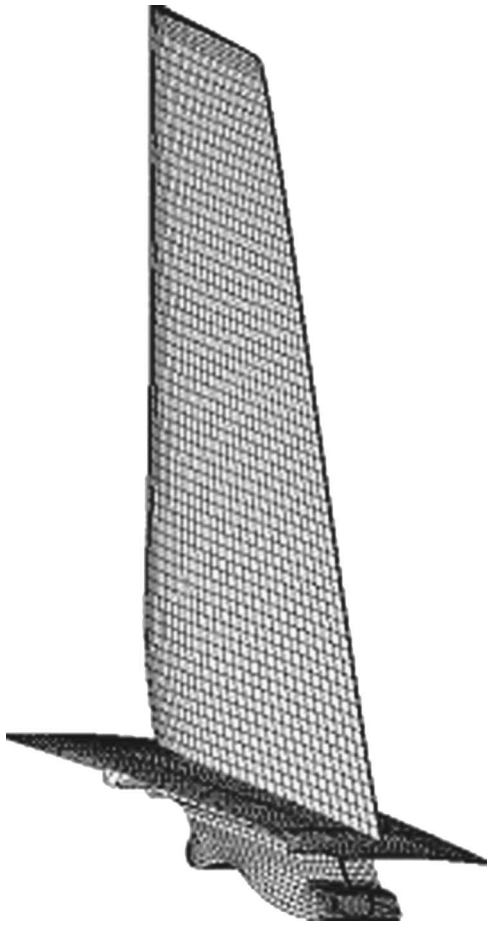

Fig. 3 Finite-element model of the blade (L=15.8 cm) with a total twist of $(\beta_R - \beta_r)$=−25 deg

Table 1 Comparison of natural frequency results computed using present analytical method versus finite-element results ($L=15.8$ cm, $a=0$, $(\beta_R-\beta_r)=-25$ deg, $c/L=0.430$)

Vibrational mode		Current analytical model		FE model with eight-noded brick elements	
Mode number	Mode shape	Nondimensional ξ	Frequency (Hz)	Frequency (Hz)	% difference
Stationary frequency (0 rpm)					
1	First flexural	3.6533	187.14	182	2.82
2	First torsion	13.8916	711.62	715	−0.47
3	Second flexural	22.8508	1170.57	1154	1.44
4	Second torsion	46.5902	2386.65	2310	3.32
5	Third flexural	61.2276	3136.47	3226	−2.78
Rotating frequency (2400 rpm)					
1	First flexural	4.1945	214.87	213	0.88
2	First torsion	13.9608	715.16	735	−2.70
3	Second flexural	23.3270	1194.96	1182	1.10
4	Second torsion	46.6035	2387.33	2350	1.59
5	Third flexural	61.7840	3164.97	3263	−3.00

the corresponding results computed by the current analytical model are shown in Table 2. It can be seen that their twisted beam FE model fails to capture the first torsional mode frequency completely.

Similarly, using the pretwisted Timoshenko beam bending equation in two directions, Banerjee [21] reports the frequencies only for the first three modes of vibration in his paper. In the sample problem to validate the results of his twisted Timoshenko beam model, Banerjee has computed these frequencies for a blade with the span-length $L=304.8$ cm, cross-sectional area $A=127.667$ cm^2, aspect ratio $(c/L)=0.667$, flexural rigidity $EI=14.3485\times10^{10}$ N cm^2, and a total twist of $(\beta_R-\beta_r)=40$ deg. The material properties for this blade such as, Young's modulus of elasticity and the mass density are $E=70$ G Pa and $\rho=2.7$ gm/cm^3, respectively. The frequencies reported by Banerjee [21] for this blade and the corresponding results computed by the current analytical model are shown in Table 2. Again, the analytical results from the current model for this particular case are in very good agreement with the maximum error limited to 3.6%.

5.3 Sample Numerical Results. For the presentation of numerical results from the current analytical model, the natural frequencies of the beam are computed in terms of nondimensional frequency parameter ξ for a very wide range of varying input parameters such as aspect ratio (c/L), total twist angle $(\beta_R-\beta_r)$, slenderness ratio $\bar{d}$, etc. These nondimensional results are shown in Figs. 4 and 5, for the untwisted and twisted beams, respectively. Figure 4 illustrates the drop in the values of nondimensional frequency parameter ξ with the increase in the aspect ratio from 0.1 (long beam) to 1.0 (square plate) for a typical value of total twist angle equal to zero (untwisted or flat beam). These values for the first two modes (first and second Flexural modes) match very well with the previous cantilever flat plate results reported by Harris and Crede [33], shown here with dotted line. The two torsion modes are also in reasonable agreement with the published data. Due to inherent limitation of the current beam model, the two-stripe vibrational mode for the flat plate shown by Harris and Crede is not picked up by the eigenvalue solution.

Figure 5 illustrates the effect of aspect ratio (c/L) variation on the changes in the values of the nondimensional frequency parameter ξ for a particular case of total twist angle of $(\beta_R-\beta_r)=45$ deg. In order to compare the results on side-by-side basis with those shown in Fig. 4, the values of the nondimensional frequency parameter ξ has been plotted for an identical range of increasing aspect ratio of (c/L) as the untwisted beam.

Table 2 Comparison of natural frequency results computed using present analytical method versus other published results for nonrotating ($\Omega=0$) twisted Timoshenko beam (Yardimoglu and Yildirim (see Ref. [20]), Banerjee (see Ref. [22]))

Vibrational mode		Current analytical model		Results from published literature	
Mode number	Mode shape	Nondimensional ξ	Frequency (Hz)	Frequency (Hz)	% difference
Yardimoglu and Yildirim[a] ($L=15.24$ cm, $\alpha=0$, $(\beta_R-\beta_r)=45$ deg, $c/L=0.167$)					
1	First flexural	3.6206	62.61	61.8	1.31
2	Second flexural	17.8910	309.38	304.8	1.50
3	First torsion	44.5846	770.98	Not shown	–
4	Twist-bend combination	55.0548	952.31	944.5	0.83
5	Third flexural	69.3112	1198.91	1193.0	0.50
Banerjee[b] ($L=304.8$ cm, $\alpha=0$, $(\beta_R-\beta_r)=40$ deg, $c/L=0.667$)					
1	First flexural	3.8123	39.42	38.05	3.60
2	First torsion	11.5461	119.39	122.51	−2.55
3	Second flexural	22.7070	234.79	226.87	3.49

[a]See Ref. [20].
[b]See Ref. [21].

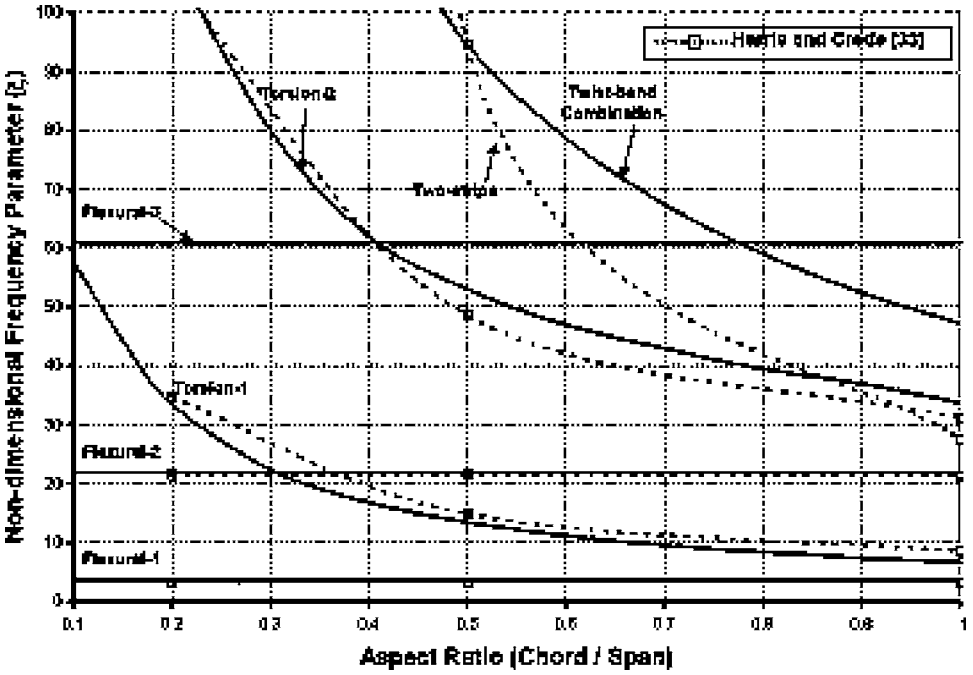

Fig. 4 Change in cantilever beam frequencies with no-twist as a function of aspect ratio (slenderness ratio=0.01)

The changes in the cantilever beam frequencies as a function of total twist angle for both stationary and rotating conditions are shown in Figs. 6–9 for aspect ratios=0.125, 0.25, 0.5, and 0.667, respectively. In these figures, we have plotted the value of nondimensional frequency parameter ξ for the first six modes. However, as the twist angle β or the aspect ratio (c/L) changes, some of the mode shapes also change as these lines cross each other. Due to these mode-crossing conditions, for example mode 2 may be first torsional mode for one twist angle, but it may become second flexural mode for some other twist angle or aspect ratio. It is observed that there is a small increase in the computed frequencies for the flexural modes as the angle of twist increases, however, the fundamental frequencies for the modes associated with the torsion about the span direction decreases rapidly with the increasing twist. In addition, the presence of centrifugal force field always tends to increase the frequencies with respect to its values in stationary condition due to stress stiffening. This trend is similar to the one observed by Hu and his co-workers [22].

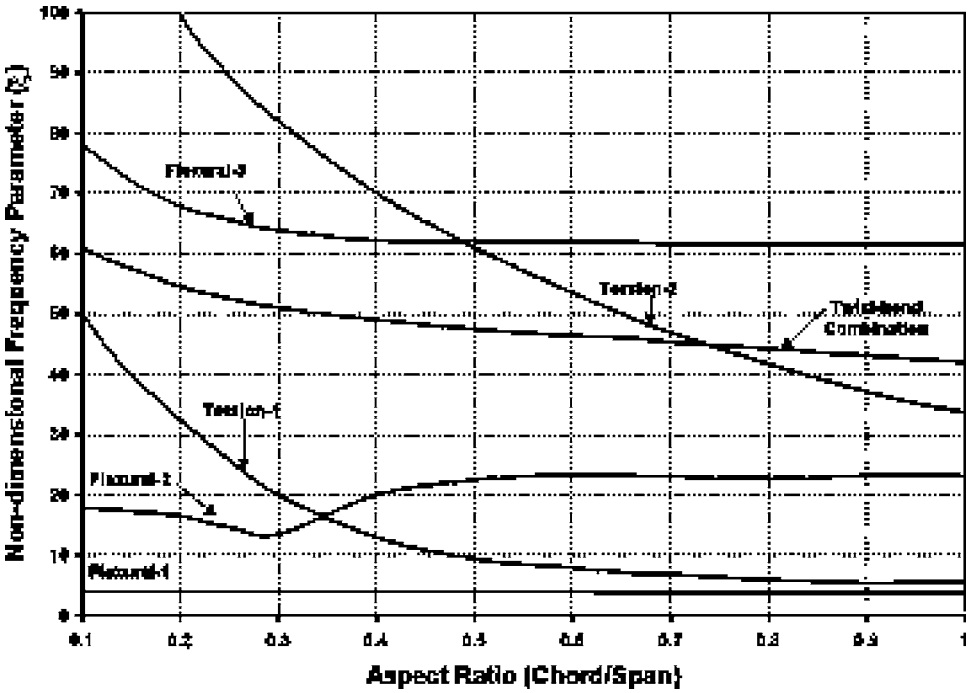

Fig. 5 Change in cantilever beam frequencies twisted at 45 deg as a function of aspect ratio (slenderness ratio=0.01)

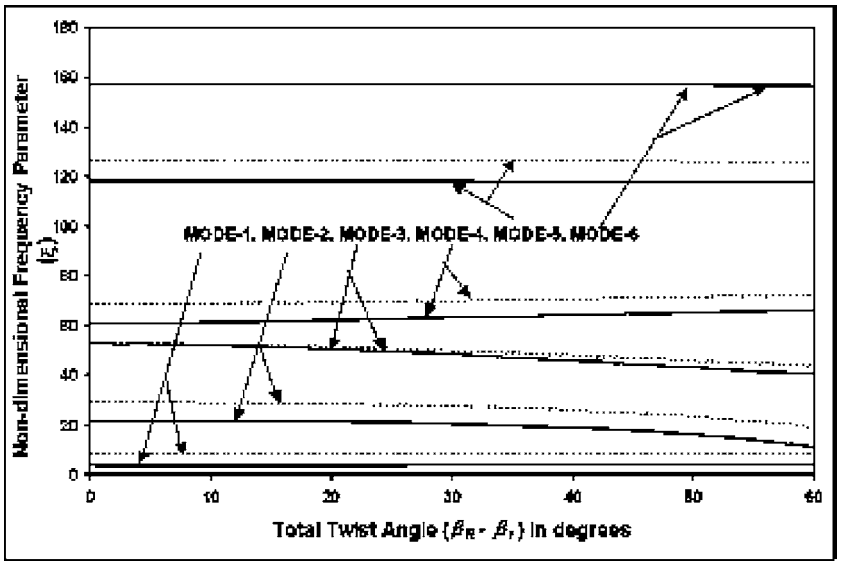

Fig. 6 Change in the twisted cantilever beam frequencies with aspect ratio (chord/span)=0.125 as a function of the total twist angle (slenderness ratio=0.01, angular velocity Ω=0.0 (stationary)—, angular velocity Ω=300 rad/s (rotating)- - -)

It should be noted that the present derivation for a pretwisted beam is completely different than other researchers' formulation [20,21,23] of using product moment of inertia terms such as, I_{yy}, I_{xy}, I_{yx}, etc. instead of torsional constant term J and shear center term (a,b). For a general asymmetric cross section such as a typical airfoil or hollow blades and turbine blades with cooling holes, the numerical computation of terms like I_{xy}, I_{yx} about the CG of the cross section is extremely cumbersome. The current approach is very convenient to analyze the dynamics of pretwisted asymmetric thin cross section such as typical airfoil blades. In addition, all the earlier researchers' derivation disregards the coupling effect of axial motion of the beam. Until now, all the axial-bending coupling investigations have been limited to axial force being treated as a buckling load on a column [23–26] rather axial motion being considered as a separate degree of freedom. The natural frequencies associated with the axial mode of vibrations (ζ degree of freedom) for the rotating Timoshenko beam have been determined and reported by the author in his previous work [9].

6 Transient Analysis Results With Contact Impact at the Free End

The transient motions caused by the periodic tip-impact load along the longitudinal axis of the beam column initiates the high-frequency axial mode of vibrations, which interacts with the low-

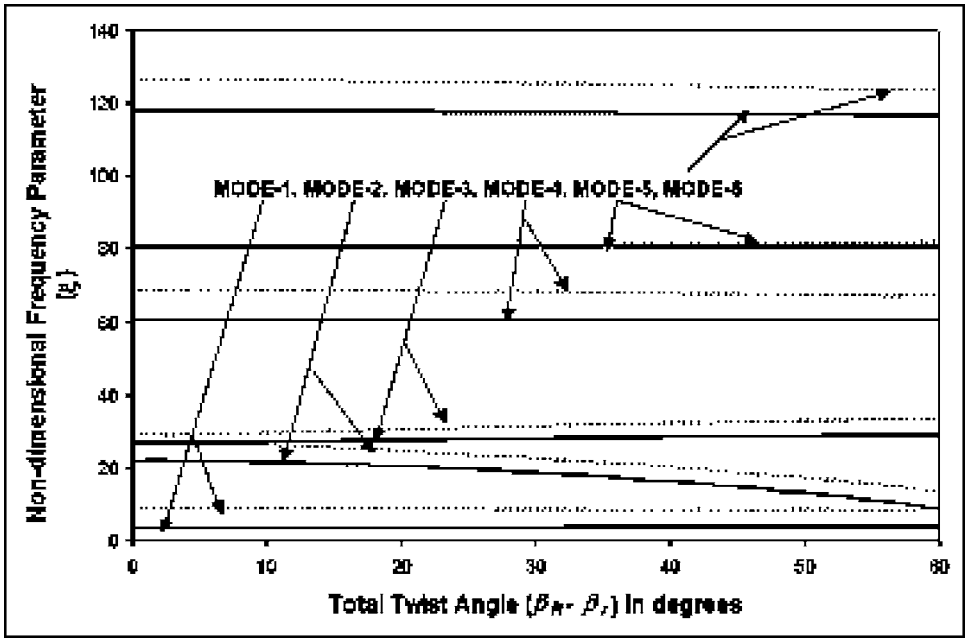

Fig. 7 Change in the twisted cantilever beam frequencies with aspect ratio (chord/span)=0.25 as a function of the total twist angle (slenderness ratio=0.01, angular velocity Ω=0.0 (stationary)—, angular velocity Ω=300 rad/s (rotating)- - -)

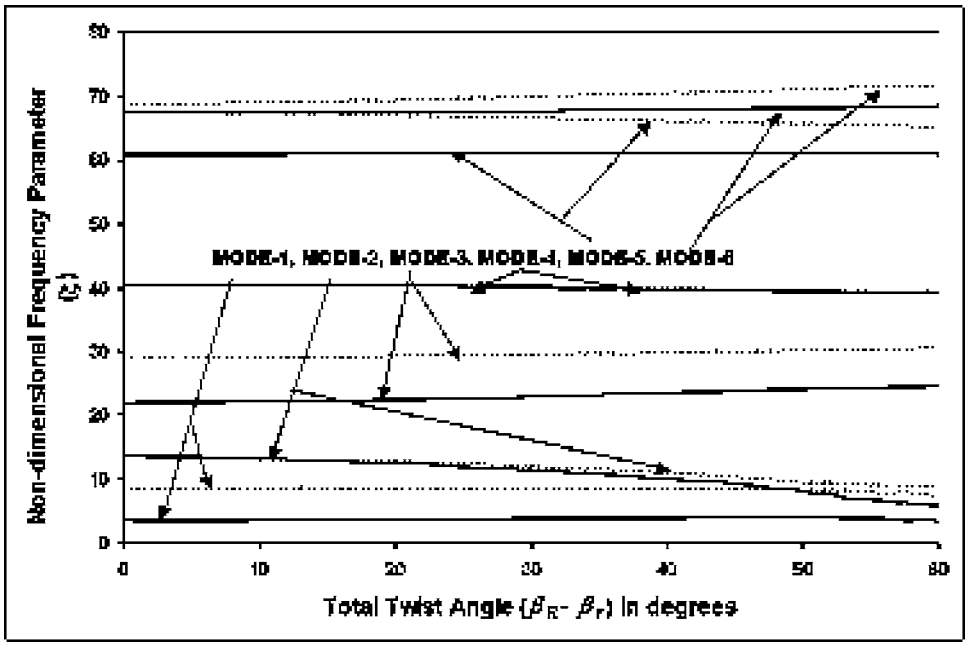

Fig. 8 Change in the twisted cantilever beam frequencies with aspect ratio (chord/span)=0.5 as a function of the total twist angle (slenderness ratio=0.01, angular velocity Ω=0.0 (stationary)—, angular velocity Ω=300 rad/s (rotating)- - -)

frequency flexural-bending mode oscillations of the beam and changes its dynamic response considerably during spin. The dynamic coupling of axial motion with the lateral deflection in a spinning beam introduces the Coriolis forces, which have very significant effect on the rub-induced vibration in a rotating machinery.

6.1 Analytically Predicted Transient Response Versus Strain Gage Data. In order to establish the accuracy of the current analytical model for its time-domain results, the numerically computed transient dynamic response of a typical high-pressure compressor blade is compared with the measured strain-gage data from a rig test [34]. In this especially developed experimental rig, it was observed that during a controlled periodic rub scenario each rub-impact produced a somewhat different transient dynamic characteristics than the one preceding rub event until the rub-induced vibration of the blade reached to a limit-cycle response under repeated rubs. For this part of the analysis using the sixth order Runge–Kutta scheme, a direct-time integration of the equations of motion outlined in Eq. (39) is performed. The aspect ratio (c/L) of the test blade is 0.659 with the span length L equal to 4 cm, and it is rotating at 16,500 rpm with the tip tangential velocity of 400 m/s. The radial lean angle is α=0 for this blade and the stagger angle is $\beta_r=\beta_R=-45$ deg. The bade tip rubs against a 72 deg circumferential rub zone with the contact-impact tip load-

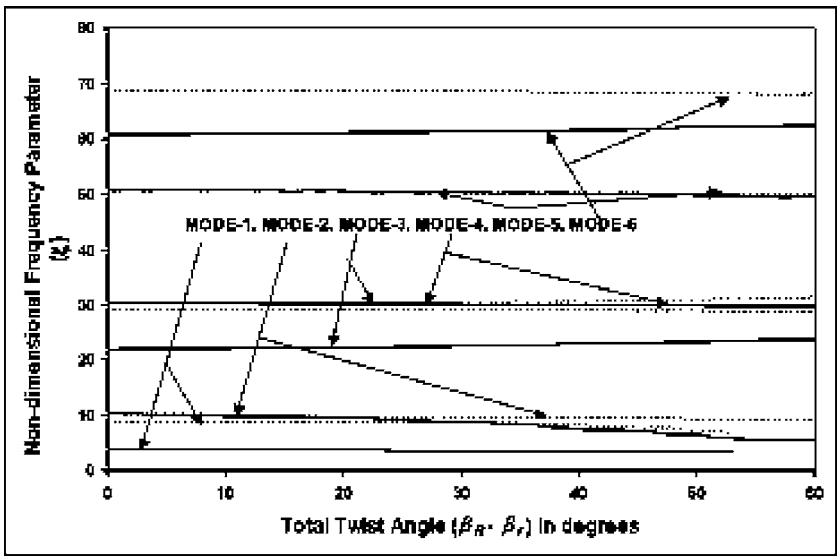

Fig. 9 Change in the twisted cantilever beam frequencies with aspect ratio (chord/span)=0.667 as a function of the total twist angle (slenderness ratio=0.01, angular velocity Ω=0.0 (stationary)——, angular velocity Ω=300 rad/s (rotating) – – –)

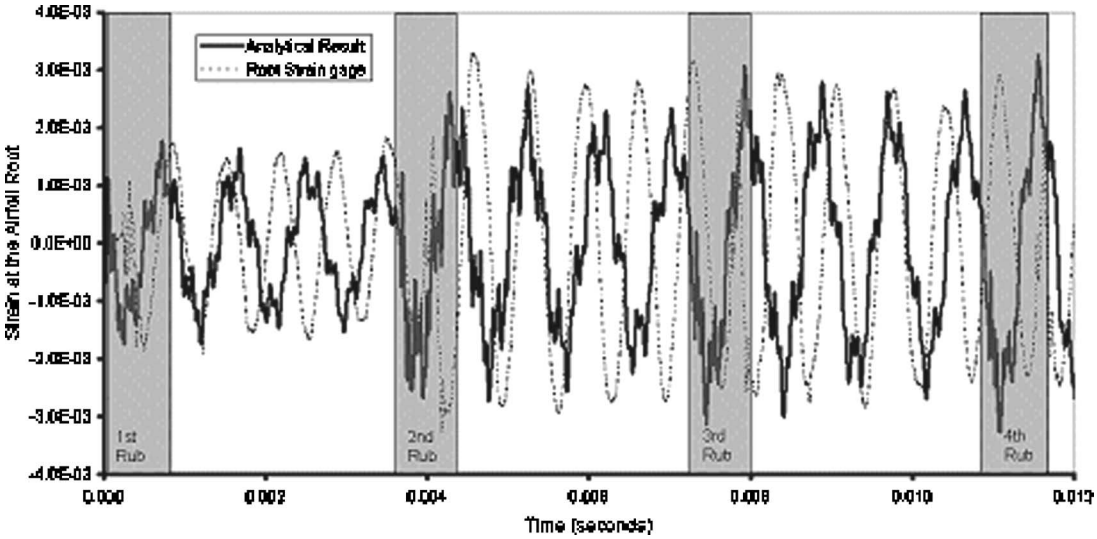

Fig. 10 Comparison of measured airfoil root strain gage data (……) versus results from the present analytical model (—) during repeated radial incursion of 0.1 mm at the blade tip with 72 deg circumferential rub zone for the first four rubs

ing applied at the rate of one pulse per revolution with 0.1 mm radial interference. In the rig test, the 72 deg forced rub zone is created by inserting a partial sector of a circumferential shoe in the path of the moving blade tip. The transient analysis has been carried out for four repeated impacts. The measured dynamic data from a spanwise strain gage at the fillet of the airfoil root is compared with the numerically computed strain time history near the clamped end of the corresponding Timoshenko beam model using the current analytical technique. From the two sets ofplotted data illustrated in Fig. 10, it can be seen that the transient analytical results predicts the dynamic characteristics and the resulting strain time history in the rubbing blade very well.

Numerically computed response shows highly nonlinear behavior of the airfoil root strains. However, in terms of frequency response, the analytical model responds at a slightly lower frequency than the test data. This can be attributed to the nonlinearity in the boundary conditions at the tip during the actual rub event. In the rig test the tip is partially constrained during the rub, whereas in the analytical model it is considered free with rub-related forces as external loads on the system. In addition, both the analytical and the test data illustrate as to how the magnitude of the response builds up after the first rub, until it stabilizes after about third rub. On this plot, the dynamic response of the blade as it passes through the 72 deg circumferential rub zone, is shown by rectangular shaded areas with legends as the first, second, third, and fourth rubs. As the spinning blade tip comes out of the forced-rub zone, the extensional wave in the blade travels up-and-down its longitudinal axis with very high velocity, giving rise to large Coriolis forces, which are oscillatory in nature. Mathematically, this Coriolis force is a distributed load; which is represented by the term such as $-2\rho A\Omega \cos \beta \zeta_{,t}$ shown in Eq. (21*b*), and its value at the blade root is computed as the integrated sum over the span length of the blade given by

$$\text{Coriolis force at the airfoil root} = -2\Omega\rho A \int_0^L \cos(\beta_r + \beta' s)\zeta_{,t} ds \tag{73}$$

The transient characteristics of this Coriolis force is shown in Fig. 11, the magnitude of which at the airfoil root could be as high as 3200 G. For this test blade, whereas the first-flex bending mode frequency is 1600 Hz, the longitudinal wave frequency is about 33,400 Hz. These longitudinal stress waves, frequency of which is more than 20 times higher than the flexural bending waves, can generate intense heat at the mating surface of the blade root (dovetail) with the disk, which has been observed to result into local welding and fretting of the mating surfaces as well as severe bearing damage even after short-duration heavy rubs. It should be noted that the decay in the magnitude of the Coriolis force, outside the imposed rub zone during the free vibration of the blade, is not due to damping in the system rather it is caused by the transfer of kinetic energy associated with the longitudinal motion into the lowest vibrational mode frequency, which invariably corresponds to its first flexural bending mode motion. The transient vibratory dynamic stresses in a rubbing airfoil is due to the interaction of longitudinal motion (hyperbolic wave) with the lateral motion (dispersive wave) of the beam, which in the case of rub-induced dynamic instability results into fatigue-type damage to the blade. Depending upon the eccentricity $(\varepsilon_c, \varepsilon_n)$ of the rub location at the blade-tip cross section, these rub-related damages can range from local tip curl due to plasticity to complete separation of the airfoil at the blade root.

6.2 Effect of Pre-twist on Transient Response During Tip-Rub. In this section, we will apply the current analytical model to investigate the transient response of a twisted blade as opposed to a similar blade but without any pretwist. For this investigation, we will use the blade parameters same as outlined in Sec. 6.1 with two different values of the total twist, that is $(\beta_R - \beta_r) = 0$ deg and $(\beta_R - \beta_r) = -45$ deg. Here, we have compared the dynamic responses of these two blades, subjected to the same contact-impact loads during a typical rub event of one pulse per revolution, in terms of their nondimensional lateral tip-deflection (η/L). The main difference of external load application between the results shown in the previous section to the current section is that the previous section results were generated for the rig-test conditions with displacement-controlled radial incursion of 0.1 mm, whereas in this section the results are for outer casing-imposed radial force of $F_{\max} = 0.1$ times of the Euler critical buckling load applied at the free end of the beam. The numerical technique to implement the controlled radial incursion or, longitudinal pulse of controlled magnitude in a transient simulation has been discussed in detail in the author's previous work [9] on the related topic. The respective results of the lateral tip-deflection (η/L) are plotted in Fig. 12.

These time-history plots up to 2.5 m s clearly show that for a

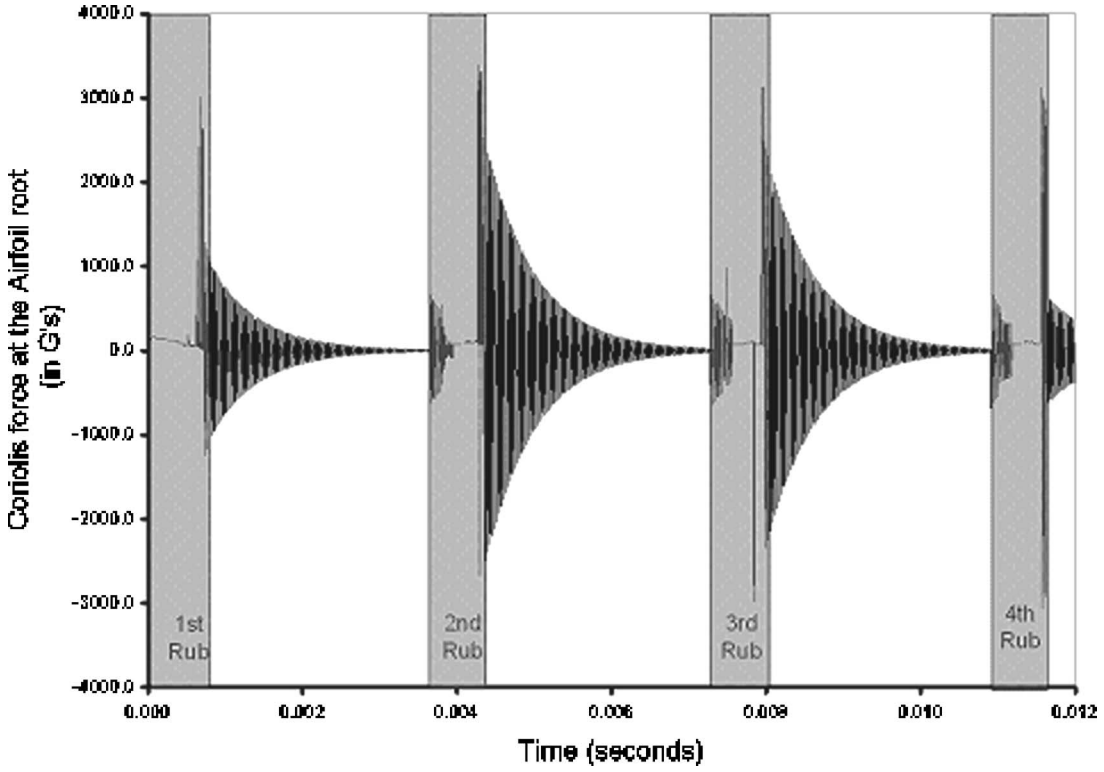

Fig. 11 Analytically computed Coriolis forces at the blade root during repeated radial incursion of 0.1 mm at the blade tip with 72 deg circumferential rub zone for the first four rubs

periodic contact-impact load of the same magnitude, the response of an untwisted blade is monotonically increasing, whereas for blade twisted at 45 deg the dynamic response shows a beating pattern. The beating pattern of a quasi-periodic nature indicates that this dynamic system is responding simultaneously at two different frequencies, which are very close to each other. It is observed that for both twisted and untwisted blades, the dynamic response until the fourth contact-impact pulse is almost identical. In addition, after each pulse loading the twisted blade responds at a slightly higher frequency than an untwisted blade.

7 Concluding Remark

The present analytical model captures the full dynamics of pretwisted cantilever Timoshenko beam with combined torsional-

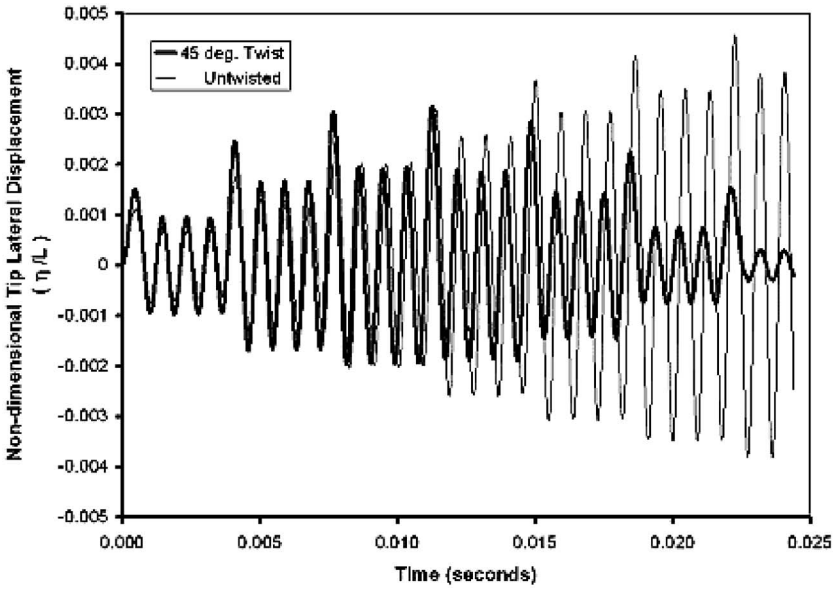

Fig. 12 Comparison of analytically computed transient lateral tip displacements for an untwisted beam (—) versus a 45 deg twisted beam (.....) during repeated rubs (one pulse per revolution) at the blade tip with a periodic contact force of magnitude F_{max}=0.1× (Euler critical buckling load)

bending-axial motion subjected to contact load F_a including Coulomb friction μ at the tip. The axial force F_a accounts for dynamic buckling effect in the event of contact-impact load at the free end. In the contact-impact scenario, the axial force F_a is a transient load represented by time-dependent function $F(t)$. As shown in the author's previous work [9] on periodic tip-pulse-loading, the general wave form of the dynamic force $F(t)$ with a frequency of $fp-Hz$ along the longitudinal axis of the Timoshenko beam can have many different time-dependent distributions, such as half-sine wave, triangular pulse, rectangular pulse, full-cosine wave with an offset, sawtooth profile, etc. The dynamic characteristics of the twisted beam are expressed by a set of four partial differential equations. These equations contain not only terms due to displacement-dependent forces rather they also include important, but very rarely derived velocity-dependent forces as well. By introducing four assumed displacement functions, the terms containing spatial coordinates s are eliminated from the equations by using Rayleigh–Ritz technique. We have formulated every term including forces due to Coriolis effect in the form of conventional $\boldsymbol{M}$, $\boldsymbol{C}$, and $\boldsymbol{K}$ matrices. The main limitation of the current beam model is its inability to obtain the classical two-stripe mode of the rotating blade. In the airfoil blade dynamics, it is well known that two-stripe mode is an important mode of vibration to be concerned, especially for short airfoils with $(c/L)\rightarrow 1$. In order to predict the two-stripe mode correctly, one must consider the coupled beam bending formulation in two planes. It is worth noting that the Timoshenko beam model developed here can be easily expanded to the more general case of coupled bending deformation in two principal planes ($x-x$ and $y-y$) as outlined in the Appendix. We would like to point out that in the coupled two-plane-bending formulation of the beam with contact-impact loading, the number of independent degrees-of-freedom in the dynamical system suddenly jumps from 4 to 6; which makes it more challenging to solve due to added complexity.

The equations of motion given in Eq. (39) are also integrated by the Runge–Kutta method to obtain the transient dynamic response in the time domain under different types of contact-impact loading at the blade tip. For accurate computing of the beam dynamic deformations associated with very high strain rates and other nonlinearities, the direct integration of equations of motion is a much preferred technique, which is also used for determining the rub-induced dynamic instability of rotating twisted blades. Using the current analytical model, we are able to predict the transient response of a rotating blade subjected to repeated rub impacts; which depending upon the contribution of various parameters such as rotational speed Ω, coefficient of friction μ, longitudinal contact load at the blade-tip F_a, load eccentricity $(\varepsilon_c, \varepsilon_n)$, etc., can make a typical rub either unstable by showing a growth in the amplitude of lateral oscillations or turn into a stable rub as a limit-cycle response.

Nomenclature

(a,b) = x-coordinate and y-coordinate of the shear center, respectively

A = cross-sectional area of the beam or blade

c = chord length of the blade airfoil cross section

$\boldsymbol{C}$ = general coefficient matrix for velocity-dependent forces

$\boldsymbol{C}_{\mathrm{D}}$ = damping matrix (symmetric)

$\boldsymbol{C}_{\mathrm{G}}$ = gyroscopic matrix (skew symmetric, causes forward and backward frequency shift in the blade)

$[C_{i,j}]$ = typical ith row and jth column term in the velocity-dependent matrix

d = depth of the blade airfoil cross section

$\bar{d}$ = slenderness ratio of the blade airfoil cross section $=\sqrt{I/AL^2}$

$(\hat{e}_a, \hat{e}_t, \hat{e}_r)$ = unit vectors in the local axial-tangential-radial system

$(\hat{e}_c, \hat{e}_n, \hat{e}_s)$ = unit vectors in the local chord-normal-span system

E = Young's modulus of elasticity of the blade or beam material

EI = flexural rigidity of the blade cross section about local x-axis (minor principal direction)

EI_{yy} = flexural rigidity of the blade cross section about local y-axis (major principal direction)

f_p = pulse frequency of the blade tip contact-load in Hz

$\boldsymbol{\mathcal{F}}$ = generalized external force vector at the blade tip

F_a = axial load on the blade (along the span direction of the blade)

F_{cf} = centrifugal force at the blade airfoil CG

F_C, F_N, F_S = components of external force vector at blade-tip $\boldsymbol{\mathcal{F}}$ due to contact

$\{f(t)\}$ = column vector containing generalized time-dependent displacement coordinates of the dynamical system

$F(t)$ = time-dependent axial load on the blade due to contact impact (along the span direction of the blade)

G = shear modulus of the blade or beam material

GJ = torsional rigidity of the thin blade cross section

I_{xx}, I_{yy} = principal moment of inertias of the blade cross section

J_o = polar moment of inertia of the blade cross section $=(I_{xx}+I_{yy})$

K_{case} = radial stiffness of the outer case filler material during rub

$\boldsymbol{K}$ = general coefficient matrix for displacement-dependent forces

$\boldsymbol{K}_F$ = in-plane force-dependent circulatory matrix due to contact force F_a

$\boldsymbol{K}_S$ = elastic stiffness matrix (symmetric)

$\boldsymbol{K}_\Omega$ = stress-stiffening or softening matrix due to spin velocity Ω

$[K_{i,j}]$ = a typical ith row and jth column term in the stiffness matrix

L = span length of the cantilever blade

$\boldsymbol{M}$ = general coefficient matrix for acceleration-dependent forces (symmetric)

$[M_{i,j}]$ = typical ith row and jth column term in the mass matrix

M = mass of the airfoil or, cantilever beam (ρAL)

$\boldsymbol{\mathcal{M}}$ = generalized external moment vector at the blade tip

M_C, M_N, M_S = components of external moment vector at blade-tip $\boldsymbol{\mathcal{M}}$ due to contact

$\{P(t)\}$ = column vector containing external forces on the dynamical system (components of this vector: $P^\psi, P^\eta, P^\zeta, P^\phi$)

$Q(s,t)$ = shear force at span location s and time t

Q_n, Q_s = distributed lateral loads on the beam in the transverse and longitudinal directions (per unit length)

R = blade tip radius

r = blade root radius or disk outer radius
s = blade local coordinates in the span direction
t = time (s)
T_c, T_s = distributed moments on the beam about the chord and longitudinal directions (per unit length)
T = total kinetic energy of the blade
U = total potential energy of the blade
$S_j(s), U_j(s), V_j(s)$ = sinusoidal shape functions for blade deformation ($j=1,2,3,\ldots,N$)
$\boldsymbol{V}$ = velocity vector of any typical point on the airfoil or beam
$W_j(t), X_j(t), Y_j(t), Z_j(t)$ = time-dependent generalized coordinates for dynamic deflection of the blade ($j=1,2,3,\ldots,N$)

Greek Symbols

α = sweep or blade lean angle with respect to the radial direction
β = blade twist or stagger angle (rad), i.e., angle between the blade chord and the engine axis (axis of rotation) at the blade tip
β_r, β_R = twist angle of the blade cross section at radii r and R
$(\beta_R - \beta_r)$ = total twist in the blade over the span length L
β' = rate of pretwist of the blade in the span direction
$\delta(s-L)$ = dirac delta unit impulse function for values at $s=L$
γ = radial clearance at the blade tip with respect to the case inner radius
$\varepsilon_c, \varepsilon_n$ = contact load eccentricity in the local chord and normal direction
ϕ, ψ, η, ζ = blade deformation due to twist, cross-section rotation, lateral deflection, and longitudinal deflections, respectively.
θ = angle of the rigid body rotation of the shaft about the spin axis at time t from time 0 ($\theta = \Omega t$ for constant angular velocity Ω)
κ = shear coefficient in the Timoshenko beam formulation
Λ = Lagrangian parameter
μ = coefficient of friction between the blade tip and the outer case
ν = Poisson's ratio of the blade material ($d\theta/dt$)
ξ = nondimensional beam frequency parameter
$\mathfrak{R}$ = rotation vector for small rotations of the airfoil cross section
χ = critical damping parameter of the blade material (nondimensional)
ω_N = natural frequency (rad/s)
Ω = blade spin velocity (rad/s)$=(d\theta/dt)$
φ_j = $(2j-1)\pi/2L$

Appendix: Effect of Beam Bending in Two Principal Directions

In the current formulation, we have considered that $I_{yy} \gg I_{xx}$, which inherently assumes that the lateral deformation in the beam will be dominated by (y-y) direction displacements. If one wants to explicitly include the deformations in the other principal direction (x-x) as well, it would result into two additional degrees-of-freedom for η and ψ. For example, in addition to twist ϕ and extension ζ of the cross section, we will have to deal with (η_y, ψ_x) due to bending about the principal (x-x) direction and (η_x, ψ_y) due to bending about the principal (y-y) direction. The resulting equations for the Timoshenko beam formulation due to fully coupled two-directional bending alone are too cumbersome to derive here and are shown in the following for reference purposes as:

(a) Bending moment balance about local (x-x) axis

$$-EI_{xx}(\psi_{x,ss}) - \kappa AG(\eta_{y,s} - \psi_x) + \beta' EI_{yy}(\beta'\psi_x) + \beta'\kappa AG\eta_x - \beta' EJ_0\psi_{y,s} - \rho I_{xx}\Omega^2\psi_x + \rho I_{xx}(\psi_{x,tt}) = T_c(s,t) \tag{A1}$$

(b) Shear force balance in the local (y-y) direction

$$-\kappa AG(\eta_{y,ss} - \psi_{x,s}) + 2\kappa AG\beta'\eta_{x,s} + \beta'^2\kappa AG\eta_y + \beta'\kappa AG\psi y - F_{cf}\cos\alpha\,\eta_{y,ss} + \rho A\,\eta_{y,tt} = Q_n(s,t) \tag{A2}$$

(c) Bending moment balance about local (y-y) axis

$$-EI_{yy}(\psi_{y,ss}) - \kappa AG(\eta_{x,s} + \psi_y) + \beta' EI_{xx}(\beta'\psi_y) + \beta'\kappa AG\eta_y + \beta' EJ_0\psi_{x,s} - \rho I_{yy}\Omega^2\psi_y + \rho I_{yy}(\psi_{y,tt}) = T_n(s,t) \tag{A3}$$

(d) Shear force balance in the local (x-x) direction

$$-\kappa AG(\eta_{x,ss} + \psi_{y,s}) - 2\kappa AG\beta'\eta_{y,s} + \beta'^2\kappa AG\eta_x + \beta'\kappa AG\psi_x - F_{cf}\cos\alpha\,\eta_{x,ss} + \rho A\,\eta_{x,tt} = Q_c(s,t) \tag{A4}$$

The corresponding new geometric boundary conditions are as follows:

$$\psi_x(0,t) = 0, \quad \eta_y(0,t) = 0, \quad \psi_y(0,t) = 0, \quad \eta_x(0,t) = 0 \tag{A5}$$

The additional four natural boundary conditions at the free end of the cantilever beam for ($s=L$) are expressed in terms of the contact-impact force vector $\boldsymbol{F}$ and moment vector $\boldsymbol{M}$ components (see Eq. (3)) as

$$(\text{Bending moment}_{xx})_{\text{at s=L}} = M_C = EI\psi_{x,s}|_{s=L} = F_a[\varepsilon_n + \varepsilon_c \sin(\beta' L)] \tag{A6}$$

$$(\text{Shear force}_{yy})_{\text{at s=L}} = F_N = -\kappa AG[\eta_{y,s} - \psi_x]_{s=L} = -\mu F_a \cos\beta_R \tag{A7}$$

$$(\text{Bending moment}_{yy})_{\text{at s=L}} = M_N = EI\psi_{y,s}|_{s=L} = -F_a[\varepsilon_c + \varepsilon_n \cos(\beta' L)] \tag{A8}$$

$$(\text{Shear force}_{xx})_{\text{at s=L}} = F_C = -\kappa AG[\eta_{x,s} - \psi_y]_{s=L} = -\mu F_a \sin\beta_R \tag{A9}$$

It should be noted that additional coupling terms will appear for the partial differential equations governing the beam motion for extension ζ and twist ϕ. Using the above equations, the interested researchers can easily expand Eqs. (21a)–(21d) to take into account of coupled bending effect about (y-y) axis.

References

[1] Carnegie, W., and Dawson, B., 1971, "Vibration Characteristics of Pre-Twisted Blades of Asymmetrical Aerofoil Cross-Section," Aeronaut. Q., **1**(3), pp. 257–273.
[2] Fu, C. C., 1974, "Computer Analysis of a Rotating Axial Turbo Machine Blade in Coupled Bending-Bending-Torsion Vibrations," Int. J. Numer. Methods Eng., **8**, pp. 569–588.
[3] Feldt, W. T., and Hermann, G., 1974, "Bending-Torsional Flutter of a Cantilevered Wing Containing a Tip Mass and Subjected to a Transverse Follower Force," J. Franklin Inst., **297**, pp. 467–478.
[4] Pigot, R., and Abel, J. M., 1975, "Vibrations and Stability of Turbine Blades at Stall," ASME J. Eng. Power, **96**, pp. 201–208.
[5] Lin, C. Y., and Chen, L. W., 2003, "Dynamic Stability of Rotating Pre-Twisted Blades with a Constrained Damping Layer," Compos. Struct., **61**, pp. 235–245.
[6] Coller, B. D., and Chamara, P. A., 2004, "Structural Non-Linearities and the

Nature of the Classic Flutter Instability," J. Sound Vib., **277**(4–5), pp. 711–739.
[7] Chen, L. W., and Peng, W. K., 1995, "Dynamic Stability of Rotating Blades With Geometric Non-Linearity," J. Sound Vib., **187**(3), pp. 421–433.
[8] Hodges, D. H., 2001, "Lateral-Torsional Flutter of a Deep Cantilever Loaded by a Lateral Follower Force at the Tip," J. Sound Vib., **247**(1), pp. 175–183.
[9] Sinha, S. K., 2005, "Non-Linear Dynamic Response of a Rotating Radial Timoshenko Beam With Periodic Pulse Loading at the Free-End," Int. J. Non-Linear Mech., **40**(1), pp. 113–149.
[10] Chen, C. K., and Ho, S. H., 1999, "Transverse Vibration of a Rotating Twisted Timoshenko Beams Under Axial Loading Using Differential Transform," Int. J. Mech. Sci., **41**, pp. 1339–1356.
[11] Timoshenko, S., Young, D. H., and Weaver, W., 1974, *Vibration Problems in Engineering*, 4th ed., Wiley, New York, pp. 432–434.
[12] Leissa, A., and Jacob, K. I., 1986, "Three-Dimensional Vibrations of Twisted Cantilevered Parallelepipeds," ASME J. Appl. Mech., **53**, pp. 614–618.
[13] Rosen, A., 1991, "Structural and Dynamic Behavior of Pretwisted Rods and Beams," Appl. Mech. Rev., **44**, pp. 483–515.
[14] Lin, S. M., Wang, W. R., and Lee, S. Y., 2001, "The Dynamic Analysis of Nonuniformly Pre-Twisted Timoshenko Beam With Elastic Boundary Conditions," Int. J. Mech. Sci., **43**, pp. 2385–2405.
[15] Petrov, E., and Geradin, M., 1998, "Finite Element Theory for Curved and Twisted Beams Based on Exact Solutions for Three Dimensional Solids. Part 1: Beam Concept and Geometrically Exact Nonlinear Formulation, Part 2: Anisotropic and Advanced Beam Models," Comput. Methods Appl. Mech. Eng., **165**, pp. 43–127.
[16] Tang, S., and Yu, A., 2004, "Generalized Variational Principle on Nonlinear Theory of Naturally Curved and Twisted Beams," Appl. Math. Comput., **153**, pp. 275–288.
[17] Lee, S. Y., and Lin, S. M., 1994, "Bending Vibrations of a Rotating Nonuniform Timoshenko Beam With an Elastically Restrained Root," ASME J. Appl. Mech., **61**, pp. 949–955.
[18] Oguamanam, D. C. D., and Heppler, G. R., 1998, "Geometric Stiffening of Timoshenko Beams," ASME J. Appl. Mech., **65**, pp. 923–929.
[19] Lin, S. M., 1999, "Dynamic Analysis of Rotating Nonuniform Timoshenko Beams With an Elastically Restrained Root," ASME J. Appl. Mech., **66**, pp. 742–748.
[20] Yardimoglu, B., and Yildirim, T., 2004, "Finite Element Model for Vibration Analysis of Pre-Twisted Timoshenko Beam," J. Sound Vib., **273**, pp. 741–754.
[21] Banerjee, J. R., 2004, "Development of an Exact Dynamic Stiffness Matrix for Free Vibration Analysis of a Twisted Timoshenko Beam," J. Sound Vib., **270**, pp. 379–401.
[22] Hu, X. X., Sakiyama, T., Matsuda, H., and Morita, C., 2004, "Fundamental Vibration of Rotating Cantilever Blades With Pre-Twist," J. Sound Vib., **271**, pp. 47–66.
[23] Chen, W. R., and Keer, L. M., 1993, "Transverse Vibration of a Rotating Twisted Timoshenko Beam Under Axial Loading," ASME J. Vibr. Acoust., **115**, pp. 285–294.
[24] Lee, H. P., 1994, "Buckling and Dynamic Stability of Spinning Pre-Twisted Beams Under Compressive Axial Loads," Int. J. Mech. Sci., **36**(11), pp. 1011–1026.
[25] Liao, C. L., and Huang, B. W., 1995, "Parametric Instability of a Spinning Pretwisted Beam Under Periodic Axial Force," Int. J. Mech. Sci., **37**(4), pp. 423–439.
[26] Sakar, G., and Sabuncu, M., 2004, "Buckling and Dynamic Stability of a Rotating Pretwisted Asymmetric Cross-Section Blade Subjected to an Axial Periodic Load," Finite Elem. Anal. Design, **40**, pp. 1399–1415.
[27] Yang, S. M., and Tsao, S. M., 1997, "Dynamics of a Pretwisted Blade Under Nonconstant Rotating Speed," Comput. Struct., **62**(4), pp. 643–651.
[28] Temel, B., and Calim, F. F., 2003, "Forced Vibration of Cylindrical Helical Rods Subjected to Impulsive Loads," ASME J. Appl. Mech., **70**, pp. 281–291.
[29] Temel, B., 2004, "Transient Analysis of Viscoelastic Helical Rods Subject to Time-Dependent Loads," Int. J. Solids Struct., **41**, pp. 1605–1624.
[30] Turhan, O., and Bulut, G., 2005, "Dynamic Stability of Rotating Blades (Beams) Eccentrically Clamped to a Shaft With Fluctuating Speed," J. Sound Vib., **280**(3–5), pp. 945–964.
[31] Timoshenko, S. P., and Goodier, J. N., 1970, *Theory of Elasticity*, 3rd ed., McGraw-Hill, New York, pp. 307–309.
[32] Timoshenko, S. P., and Gere, J. M., 1961, *Theory of Elastic Stability*, 2nd ed., McGraw-Hill, New York, pp. 212–250.
[33] Harris, C. M., and Crede, C. E., 1976, *Shock and Vibration Handbook*, 2nd ed., McGraw-Hill, New York, pp. 7–14.
[34] Padova, S., Barton, J., Dunn, M. G., Manwaring, S., Young, G., Adams, M., Jr., and Adams, M., 2004, "Development of an Experimental Capability to Produce Controlled Blade Tip/Shroud Rubs at Engine Speed," *Proceedings of IGTI: ASME/IGTI Turbo Expo 2004*, Vienna, Austria, June 14–17, Paper No. GT2004-53322.